Atmos. Chem. Phys. Discuss., 14, 14519–14573, 2014
www.atmos-chem-phys-discuss.net/14/14519/2014/
doi:10.5194/acpd-14-14519-2014

Atmospheric Chemistry and Physics Discussions

Evaluation of OMI operational standard NO_2 column retrievals using in situ and surface-based NO_2 observations

L. N. Lamsal[1,2], N. A. Krotkov[2], E. A. Celarier[1,2], W. H. Swartz[3,2], K. E. Pickering[2], E. J. Bucsela[4], R. V. Martin[5,6], S. Philip[5], H. Irie[7], A. Cede[8,2], J. Herman[9,2], A. Weinheimer[10], J. J. Szykman[11], and T. N. Knepp[12,13]

[1]Goddard Earth Sciences Technology and Research, Universities Space Research Association, Columbia, MD 21046, USA
[2]NASA Goddard Space Flight Center, Greenbelt, MD 20771, USA
[3]Applied Physics Laboratory, the Johns Hopkins University, Laurel, MD 20723, USA
[4]SRI International, Menlo Park, CA 94025, USA
[5]Department of Physics and Atmospheric Science, Dalhousie University, Halifax, NS, B3H 3J5, Canada
[6]Harvard-Smithsonian Center for Astrophysics, Cambridge, MA, USA
[7]Center for Environmental Remote Sensing, Chiba University, 1-33, Yayoicho, Inage-ku, Chiba 263-8522, Japan
[8]LuftBlick, Kreith, Austria

[9]University of Maryland, Joint Center for Earth Systems Technology, Baltimore, MD 21228, USA
[10]National Center for Atmospheric Research, Boulder, CO 80307, USA
[11]United States Environmental Protection Agency Office of Research and Development, Hampton, VA 23681, USA
[12]Science Systems and Applications, Inc., Hampton, VA 23681, USA
[13]NASA Langley Research Center, Hampton, VA 23681, USA

Received: 31 March 2014 – Accepted: 19 May 2014 – Published: 5 June 2014

Correspondence to: L. N. Lamsal (lok.lamsal@nasa.gov)

Published by Copernicus Publications on behalf of the European Geosciences Union.

ACPD
14, 14519–14573, 2014

Abstract

We assess the standard operational nitrogen dioxide (NO_2) data product (OMNO2, version 2.1) retrieved from the Ozone Monitoring Instrument (OMI) onboard NASA's Aura satellite using a combination of aircraft and surface in situ measurements as well as ground-based column measurements at several locations and a bottom-up NO_x emission inventory over the continental US. Despite considerable sampling differences, NO_2 vertical column densities from OMI are modestly correlated ($r = 0.3$–0.8) with in situ measurements of tropospheric NO_2 from aircraft, ground-based observations of NO_2 columns from MAX-DOAS and Pandora instruments, in situ surface NO_2 measurements from photolytic converter instruments, and a bottom-up NO_x emission inventory. Overall, OMI retrievals tend to be lower in urban regions and higher in remote areas, but generally agree with other measurements to within ± 20 %. No consistent seasonal bias is evident. Contrasting results between different data sets reveal complexities behind NO_2 validation. Monthly mean vertical NO_2 profile shapes from the Global Modeling Initiative (GMI) chemistry-transport model (CTM) used in the OMI retrievals are highly consistent with in situ aircraft measurements, but these measured profiles exhibit considerable day-to-day variation, affecting the retrieved daily NO_2 columns by up to 40 %. This assessment of OMI tropospheric NO_2 columns, together with the comparison of OMI-retrieved and model-simulated NO_2 columns, could offer diagnostic evaluation of the model.

1 Introduction

Nitrogen oxides ($NO_x = NO + NO_2$) play a key role in atmospheric chemistry by controlling the production of tropospheric ozone, forming aerosol nitrates, and affecting the abundance of the hydroxyl radical (OH) and the lifetimes of greenhouse gases (Solomon et al., 1999; Intergovernmental Panel on Climate Change, 2007). Nitrogen dioxide (NO_2) is one of the pollutants regulated by the Environmental Protection

ACPD
14, 14519–14573, 2014

Agency (EPA), as it is detrimental to human health and ecosystems (EPA, 2009). Major sources of NO_x include combustion, soil emissions, and lighting. Tropospheric NO_2 concentrations are highly variable in space and time due to spatial heterogeneity of NO_x sources and the relatively short lifetime of NO_x in the lower troposphere.

NO_2 is measured locally by in situ monitors and detected remotely in an atmospheric column by ground-based and satellite instruments. NO_2 observations from satellite offer a globally consistent data set, albeit at coarse resolutions of 10 s to 100 s of kilometers, enabling a wide range of applications including many not feasible from in situ observations. Several studies have used satellite observations of NO_2 to evaluate chemical transport models (Martin et al., 2002; van Noije et al., 2006; Lamsal et al., 2008; Kim et al., 2009; Herron-Thorpe et al., 2010; Huijnen et al., 2010), examine spatial and temporal patterns of NO_x emissions (Beirle et al., 2003; Richter et al., 2005; Kim et al., 2006; van der A et al., 2006; Zhang et al., 2007; Boersma et al., 2008a; Lu and Streets, 2012; Wang et al., 2012; Hilboll et al., 2013; Russell et al., 2010, 2012; Duncan et al., 2013), examine NO_x sources (Jaeglé et al., 2005; van der A et al., 2008; Bucsela et al., 2010; de Wildt et al., 2012; Lin, 2012; Ghude et al., 2010, 2013a; Mebust et al., 2011; Mebust and Cohen, 2013), provide top-down constraints on surface NO_x emissions (Martin et al., 2003; Konovalov et al., 2006; Zhao and Wang, 2009; Lin et al., 2010; Lamsal et al., 2011; Ghude et al., 2013b; Vinken et al., 2014), infer NO_x lifetimes (Schaub et al., 2007; Lamsal et al., 2010; Beirle et al., 2011), and estimate surface NO_2 concentrations (Lamsal et al., 2008, 2013; Novotny et al., 2011; Bechle et al., 2013). The quality of the satellite data directly affects every one of these applications and estimates. Careful assessments of the accuracy of retrievals with credible, coincident, independent measurements help ensure reliable analyses.

Tropospheric NO_2 column retrievals from satellites have been evaluated with in situ NO_2 profile measurements from aircraft (Heland et al., 2002; Martin et al., 2006; Boersma et al., 2008a; Bucsela et al., 2008, 2013; Celarier et al., 2008; Hains et al., 2010), NO_2 column measurements from ground-based and airborne instruments (Ionov et al., 2008; Celarier et al., 2008; Brinksma et al., 2008; Kramer et al., 2008; Irie

ACPD
14, 14519–14573, 2014

et al., 2008, 2012; Wenig et al., 2008; Oetjen et al., 2013), in situ surface measurements (Schaub et al., 2006; Blond et al., 2007; Boersma et al., 2009; Lamsal et al., 2008, 2010), and a bottom-up NO_x emission inventory (Lamsal et al., 2010). Aircraft offer precise in situ measurements within vertical spirals covering a spatial domain over a satellite field of view, but these are generally campaign-based experiments spanning only a few days to weeks and are limited by the need to extrapolate below the lowest measurement altitude (e.g. Bucsela et al., 2008). Ground-based NO_2 column observations from the Multi-AXis Differential Optical Absorption Spectroscopy (MAX-DOAS) and direct-sun DOAS are maturing, but assessments with these measurements are still restricted by a limited number of sites. Validation with in situ surface NO_2 measurements from dense networks of commercial molybdenum converter analyzers are complicated by instrument interferents (e.g. Steinbacher et al., 2007; Lamsal et al., 2008), and is more appropriate in rural areas (Lamsal et al., 2010). Observations of NO_2 from photolytic converter analyzers (Ryerson et al., 2000) are sparse, but offer useful opportunities to evaluate satellite retrievals. In the United States, the confidence in the estimates of local and regional emissions are at medium to high levels, suggesting low uncertainty in total continental NO_x emissions (NARSTO, 2005). Validation using the US emission data benefits from a large domain coincident with satellite observations and a variety of observational conditions. This study takes advantage of state-of-the-art NO_2 measurement technique, and exploits the strength of various measurements to assess the quality of the new standard tropospheric NO_2 retrievals (OMNO2, version 2.1) from the Ozone Monitoring Instrument (OMI) under various atmospheric conditions.

Well-validated daily global observations from satellite provide a rich resource to evaluate results from regional air quality (AQ) models and global chemical transport models (CTMs), thereby helping to increase model accuracy. To facilitate satellite-model comparison, the OMNO2 product provides information on vertical NO_2 measurement sensitivity (scattering weights). Combining scattering weights with model-derived vertical NO_2 profile shape allows for the calculation of new air mass factors (AMFs) needed

ACPD
14, 14519–14573, 2014

to convert satellite-retrieved slant column densities (SCDs) to vertical column densities (VCDs). Since the assumed vertical distribution of NO_2 in the retrieval is taken from the model subject to evaluation, this approach allows consistent comparison of satellite-observed columns with model-simulated columns. Applying a similar approach for in situ NO_2 measurements from aircraft provides insights into the retrieval uncertainty, as using measured profiles and resulting AMFs indicate how much the satellite retrieval would change when climatological assumptions about profile shape are replaced with specific, observed profile information.

Our main goals here are to assess the operational OMI NO_2 standard product, elucidate errors in retrieved columns due to a priori NO_2 vertical profiles through the use of nearly-coincident NO_2 profiles measured from aircraft, and devise objective methods to compare model-simulated NO_2 columns with satellite retrievals. Section 2 describes the OMI retrievals and various concurrent data sources used in this study. We present validation results in Sect. 3. The impacts of the a priori NO_2 profiles used in the satellite retrievals are discussed in Sect. 4. We discuss the comparison of modeled and OMI NO_2 in Sect. 5. Section 6 summarizes the conclusions of this study.

2 Observations

2.1 OMI retrieval

The Dutch-Finnish OMI instrument aboard the NASA EOS-Aura satellite provides continuous monitoring of atmospheric NO_2 columns through measurement of hyperspectral solar backscatter in the UV-visible range from 264 to 504 nm (Levelt et al., 2006). The satellite was launched on 15 July 2004, into a polar, sun-synchronous orbit with an equator-crossing time of 13:45 LT (ascending node). OMI observes the atmosphere in 60 cross-track ground pixels measuring 13–26 km along track and 24–128 km across track, achieving daily global coverage.

ACPD
14, 14519–14573, 2014

We use the tropospheric NO_2 columns from OMI standard product (Bucsela et al., 2013) publicly available from the NASA archive: http://disc.sci.gsfc.nasa.gov/Aura/data-holdings/OMI/omno2_v003.shtml. The algorithm uses the Differential Absorption Spectroscopy (DOAS) technique (Platt, 1994) to determine NO_2 SCD by nonlinear least squares fitting of reference spectra for NO_2, ozone, H_2O and the Ring filling-in effect to the OMI-measured reflectance in the 405–465 nm spectral window (Bucsela et al., 2006; Boersma et al., 2007). The slant column represents the integrated NO_2 abundance along the average light path from the Sun, through the atmosphere, to the satellite. The measured SCDs are corrected for instrumental artifacts (stripes Dobber et al., 2008; Bucsela et al., 2013) accounting for cross-track variation of the stratospheric AMF. The AMF, defined as the ratio of the SCD to the VCD, is calculated using a look-up table of vertically resolved NO_2 sensitivities (scattering weights) and various input parameters including viewing geometry, surface reflectivity, effective cloud pressure, cloud radiance fraction, and a priori NO_2 vertical profile shapes (Palmer et al., 2001). The a priori NO_2 profiles are early afternoon (at the OMI overpass time) monthly mean values derived from the Global Modeling Initiative (GMI at $2^\circ \times 2.5^\circ$) CTM (Appendix A) (Strahan et al., 2007). To separate stratospheric and tropospheric columns, the algorithm first applies stratospheric (close to geometric) AMFs to the de-striped measured SCDs to yield initial VCDs. Cloud-free areas of tropospheric contamination in the stratospheric NO_2 field are identified using the a priori GMI monthly mean tropospheric NO_2 columns and OMI cloud measurements. Those regions are then masked and filled in with the stratospheric VCDs measured outside the masked regions, primarily from unpolluted or cloudy areas. The stratospheric field is further smoothed by using a boxcar averaging.

The uncertainties in the retrieval of tropospheric NO_2 columns arise from the uncertainties in the retrieval of slant column densities, the calculation of AMFs, and the separation of stratospheric and troposphere components. The uncertainty in the individual OMI NO_2 slant column is $\sim 0.75 \times 10^{15}$ molec. cm^{-2} (Boersma et al., 2004, 2011; Bucsela et al., 2013) and dominates the overall retrieval error over the oceans and remote

ACPD
14, 14519–14573, 2014

areas. AMF uncertainties are ~ 20 % in clear-sky and 30–80 % under cloudy conditions and dominate overall retrieval errors over continental polluted regions. The uncertainty in the stratosphere–troposphere separation is rather small at 0.20×10^{15} molec. cm^{-2} (Bucsela et al., 2013). In this study, we include the data for scenes with cloud radiance fractions less than 0.5 and those unaffected by the OMI row anomaly (Dobber et al., 2008).

2.2 In situ NO_2 measurements from aircraft

In situ NO_2 concentrations were measured from the NASA P-3B aircraft in the Baltimore-Washington, D.C. metropolitan region on 14 flight days in July 2011, as part of the NASA Earth Venture-1 DISCOVER-AQ (Deriving Information on Surface Conditions from Column and Vertically Resolved Observations Relevant to Air Quality) field program (Crawford et al., 2014). Measurements usually began between 7:00 and 10:00 local time and continued for about 8 h. Flights occurred over a range of weather conditions including clean days, pollution episodes, and weekdays and weekends. The P-3B aircraft housed two well-characterized in situ NO_2 measuring instruments: The University of California, Berkeley thermal dissociation laser induced fluorescence (TD-LIF, (Thornton et al., 2000; Wagner et al., 2011) and the National Center for Atmospheric Research (NCAR) 4-channel chemiluminescence instrument (P-CL). The P-CL measures NO_2 by photolysis of NO_2 and chemiluminescence detection of the product NO (Ridley and Grahek, 1990; Ridley et al., 2004). The TD-LIF instrument had a low NO_2 sampling frequency due to an alternating measurement cycle for other species such as peroxynitrates, alkylnitrates, and nitric acid, so we use measurements from the NCAR P-CL. The instrument has an NO_2 measurement uncertainty of 10 % and a 1 s, 2σ detection limit of 50 ppt, making it useful to measure NO_2 in the free troposphere.

Figure 1 shows a typical in situ NO_2 measurement pattern during DISCOVER-AQ. Flight tracks for this campaign targeted urban air pollution spatially along the Interstate 95 (I-95) corridor in the Baltimore-Washington, D.C. region and vertically over the Chesapeake Bay and six surface air quality monitoring sites (see Table 1). Typi-

ACPD
14, 14519–14573, 2014

cally, during each sortie, three vertical spirals were flown over each location, covering altitudes from ~ 300 m, in the boundary layer to ~ 3.3 km, in the free troposphere. Table 1 provides the details on the number of spirals and observations and the measured altitude range. There were a total of 13–19 P-3B spirals over each surface site with 5356–15 827 1 s observations made near the time of the OMI overpass. We found that the limited vertical extent of the aircraft pass over I-95 and the Chesapeake rendered those measurements less useful. We binned the measurements to the pressure grid of the GMI model to directly compare the model profiles with observed profiles, and to estimate the retrieval error due to the difference.

Figures 1 and 2 show the early afternoon (12:00–15:00) NO_2 vertical profiles measured during DISCOVER-AQ. NO_2 mixing ratios over land range over 0.02–28 ppb below 950 hPa, decrease sharply to 0.01–2 ppb at ~ 800 hPa, and are 10–200 ppt above 700 hPa. Over the Chesapeake Bay, NO_2 mixing ratios are generally less than 1 ppb, and the vertical gradient in the profile is less pronounced due to limited surface sources and transported NO_2 downwind. Large spatial and temporal variability in near-surface NO_2 reflect the large spatiotemporal variation in NO_x emissions and differences in local dynamics. NO_2 enhancement and variability over Beltsville and Essex are largely due to local emissions, mostly from traffic. Most sites experienced more than factor-of-two greater NO_2 concentrations on highly polluted days with a shallow mixed layer on 5, 10, 21, and 28 July.

The aircraft measurements show that NO_2 concentrations within the mixed layer make the largest contributions to tropospheric NO_2 columns. The lowest 1 km of sampled aircraft data contain 64–84 % of the NO_2 column below 5 km. The same altitude range in the GMI profile represents 72–83 %, providing confidence in the GMI simulation. In the free troposphere (2–5 km), NO_2 concentrations from the a priori GMI climatology and aircraft measurements generally agree to within 0.03 ppb. GMI simulations suggest that the NO_2 partial column within first few hundred meters from the ground to the lowest aircraft altitude comprise 30–40 % of the total column. The upper tropospheric column above 5 km is rather small, consisting of 10–15 % of the total column.

ACPD
14, 14519–14573, 2014

We inferred the complete P-3B tropospheric NO_2 column by combining the measured values with GMI climatology above the highest aircraft level and extrapolating below the lowest aircraft level. The extrapolation scheme applies the vertical gradient of the NO_2 concentrations between the lowest aircraft altitude (C_M^j) and underneath (C_M^{j-1}) in the GMI profiles to the measured concentration (C^j) to estimate concentration (C^{j-1}):

$$C^{j-1} = \frac{C_M^{j-1}}{C_M^j} \times C^j, \quad (1)$$

where the subscript "M" represents model. In this approach, we assume that the GMI model captures the vertical distribution of NO_2 well. Errors in the calculated gradient propagate into the extrapolated value, degrading the quality of integrated P-3B tropospheric NO_2 columns. Allowing factor-of-two extrapolation errors, the errors in the integrated P-3B tropospheric NO_2 columns are generally less than 20 %.

2.3 Ground-based MAX-DOAS

Tropospheric NO_2 columns were measured by the ground-based MAX-DOAS instruments for several months during 2006–2011 at a remote site in Hedo and a suburban site in Tsukuba, Japan. NO_2 observations at these sites allow us to assess the OMI retrievals for contrasting environments (rural vs. urban).

The MAX-DOAS instrument measures scattered sunlight observations in the UV/visible wavelengths at several elevation angles between the horizon and zenith (e.g. Hönninger et al., 2004; Irie et al., 2012). Spectral fitting of the MAX-DOAS measured differential structure with absorption cross-section of NO_2 from Vandaele et al. (1998) at 294 K and other interfering species including O_2–O_2, O_3, H_2O, and the Ring and undersampling effects over the 460–490 nm window yields the differential slant column density, i.e., the difference in integrated columns along the average light path between measurements made at low elevation angles and that at an elevation angle of 90°. The

ACPD
14, 14519–14573, 2014

accuracy of the retrieved NO_2 slant columns is ~ 10 %, as confirmed by a formal semi-blind intercomparison experiment involving MAX-DOAS observations from different research groups (Roscoe et al., 2010). The NO_2 slant column densities are converted to tropospheric vertical column density by using the AMF calculated with measured aerosol information and the vertical profile of NO_2 and a non-linear iterative inversion scheme (Irie et al., 2012). Additional details on the MAX-DOAS measurements, calibration, and retrieval procedures can be found in Irie et al. (2008) and references therein. Overall errors in the tropospheric NO_2 vertical columns are < 14 %.

The MAX-DOAS instrument observes air masses representative of horizontal distance of about 10 km (Irie et al., 2012), comparable to the OMI spatial resolution. The temporal resolution corresponds to a complete sequence of elevation angles lasting for 30 min. We use the MAX-DOAS measurements taken within 30 min of OMI overpasses to compare with the OMI retrievals.

2.4 Ground-based Pandora

The direct sun total NO_2 column measurements were carried out at 12 DISCOVER-AQ sites (including six aircraft spiral locations) in Maryland and at the Chemistry and Physics Atmospheric Boundary Layer Experiment (CAPABLE) site at NASA's Langley Research Center in Hampton, Virginia. The CAPABLE site is located in a coastal suburban area, which could experience sporadic local and transported NO_x emissions. Additional details on the CAPABLE site can be found in Knepp et al. (2013). These measurements are useful to examine spatial and temporal variation in the OMI retrievals.

Pandora is a ground-based spectrometer that measures direct solar irradiance over the range 280–525 nm at the spectral resolution of 0.6 nm, allowing the retrieval of the total column abundance of various species, such as O_3, NO_2, HCHO, H_2O, and SO_2 (Herman et al., 2009). An algorithm for the retrieval of NO_2 from Pandora is similar to the direct-sun NO_2 inversion method from a Brewer spectrometer (Cede et al., 2006). The direct-sun DOAS technique is equally sensitive to stratospheric and tropospheric

ACPD
14, 14519–14573, 2014

NO_2, and is not affected by the Ring effect. The algorithm initially retrieves the relative NO_2 slant columns by least-square fitting of the difference between the logarithm of a reference irradiance spectrum and the logarithm of measured irradiance spectra with the absorption spectra of NO_2 (Vandaele et al., 1998) and other atmospheric absorbers, a low-order polynomial, and wavelength shift and squeeze functions in the spectral range 370–500 nm. The differential NO_2 slant columns represent the difference between the absolute slant columns in the measured and the reference spectrum used for normalization. The reference spectrum is an average spectrum measured on clear clean days. The absolute slant column in the reference spectrum is determined by the Minimum-Amount Langley-Extrapolation method, as described in Herman et al. (2009). The direct sun AMF can be approximated as the secant of solar zenith angle and therefore does not require radiative transfer calculations or prior knowledge of the ground reflectivity or NO_2 profile shape.

The Pandora spectrometer provides NO_2 vertical column observations with a clear-sky precision of about 2.7×10^{14} molec. cm^{-2} and a absolute accuracy of 2.7×10^{15} molec. cm^{-2}. NO_2 column retrievals from Pandora have been previously validated against direct-sun Multi-Function DOAS (MFDOAS) and Fourier Transform Ultraviolet Spectrometer (UVFTS) data and have been found to agree to within 12 % (Piters et al., 2012; Wang et al., 2010; Herman et al., 2009). Here, we compute 30 min Pandora column averages close to the OMI overpass time to compare with the nearest OMI NO_2 columns representing individual field of view (FOV). The maximum allowed collocation radius (distance between the center of the OMI FOV and the Pandora site) is 10 km.

2.5 In situ surface measurements

In situ measurements of surface NO_2 were made at the South Eastern Aerosol Research and CHaracterization (SEARCH) network, consisting of 7 sites in the Southeastern United States (Edgerton et al., 2006). We use data from two regionally representative sites: Centreville, in Alabama, and Yorkville, in Georgia measured during 2006–2009. NO_2 measurements are made using photolytic converter analyzers,

ACPD
14, 14519–14573, 2014

a measurement method that employs photolysis of ambient NO_2 followed by chemiluminescence detection of the product NO. This method offers highly accurate NO_2 measurements, with an uncertainty < 10 %.

3 Evaluation of the OMI retrieval

3.1 NO_2 profile shapes

We initially evaluate the a priori monthly mean relative vertical distribution (shape factor) of NO_2 used in the OMI NO_2 retrievals with aircraft measurements during the DISCOVER-AQ field campaign. Figure 3 compares average NO_2 shape factors over various locations from aircraft with those calculated with the GMI model. Although the aircraft measurements are qualitatively similar to the model results, differences up to 30 % were observed near the surface and in the free-troposphere. Both the measurements and the model suggest that 20–30 % of the tropospheric NO_2 column is located near the surface (first model layer, ~ 1000 hPa), while only 5–10 % is in the mixed layers between 900–1000 hPa, and less than 3 % is in the free-troposphere (< 900 hPa). Aircraft measurements indicate the horizontal spatial gradient in the free-tropospheric shape factors, primarily due to the dominant lower tropospheric contributions to the total tropospheric NO_2 columns in urban source regions. Day-to-day variations in aircraft NO_2 shape factors are up to a factor of two.

3.2 Tropospheric NO_2 columns

3.2.1 Comparison with in situ aircraft measurements

In this section, we compare OMI tropospheric NO_2 columns with integrated columns from aircraft spirals at six locations in Maryland during the DISCOVER-AQ field campaign in July 2011. We select only the spirals made within 1 h of the OMI overpass.

ACPD
14, 14519–14573, 2014

Not all data from the 14 flight days could be used due to adverse instrumental (row anomaly) or cloudy conditions affecting the OMI data.

Figure 4 shows tropospheric NO_2 columns from OMI and vertically integrated in situ aircraft measurements for several individual flight days. OMI and the in situ tropospheric NO_2 columns exhibit moderate correlation, with a mean correlation coefficient of 0.4 and a maximum value of 0.7. Individual measurements agree to within 20 % in 60 % of cases at Fair Hill, Aldino, Padonia, and Beltsville. A more substantial difference was observed at Edgewood and Essex, where aircraft measurements were systematically higher than OMI retrievals. These two coastal towns were often impacted by a bay breeze, yielding complex vertical and horizontal distributions of NO_2. The observed discrepancy between the two measurements is primarily due to the difference in spatial sampling, but it could also be due to other reasons, such as errors in OMI tropospheric NO_2 due to inaccurate removal of stratospheric NO_2 on 2 July and partly cloudy conditions obstructing the scene on 20 July.

Figure 5 shows the campaign average tropospheric NO_2 columns observed by the OMI and aircraft instruments. Measurements from both instruments exhibit a distinct spatial variation, with low columns at the rural site Fair Hill and high columns in urban sites such as Beltsville and Essex. NO_2 retrievals from OMI are lower than aircraft measurements by 5.8–22.1 %, with the exception of Edgewood and Essex, where aircraft measurements are often up to a factor of two higher than OMI retrievals. We quantify the impact of the a priori NO_2 profiles in the OMI retrievals for the observed discrepancy between OMI and in situ measurements in Sect. 4.

3.2.2 Comparison with Pandora measurements

We compare OMI total NO_2 columns (sum of tropospheric and stratospheric columns) with Pandora direct sun NO_2 column retrievals at six sites in Maryland during the first DISCOVER-AQ field campaign in July 2011 and at the CAPABLE site at NASA Langley in Hampton, Virginia for 2010–2012. Although analysis of Pandora measurements allows inference of the stratospheric portion of the total NO_2 column (Herman et al.,

ACPD
14, 14519–14573, 2014

2009), the separate stratospheric and tropospheric components are not currently available from Pandora. Subtraction of OMI-derived stratospheric NO_2 columns from Pandora total column measurements could as well introduce errors in Pandora-derived tropospheric NO_2 columns. Therefore the use of total columns allows us to reduce these errors, and allows more direct comparison between the two measurements.

Figure 6 presents a comparison of coincident total NO_2 column retrievals from the OMI and Pandora instruments. The variations of OMI NO_2 are broadly consistent with the Pandora measurements. Although the OMI and Pandora NO_2 columns are modestly correlated ($r < 0.54$), they generally agree to within 18 % at Aldino and Beltsville and within 30 % at the other DISCOVER-AQ sites. Occasional large discrepancies are evident, reflecting a combination of enhanced spatial variation and placement of the Pandora spectrometers.

Figure 5 shows campaign average total NO_2 columns measured by Pandora and OMI at six DISCOVER-AQ sites in Maryland. The measurements are in good agreement. NO_2 columns measured with the Pandora are on average < 6 % higher at Aldino, Beltsville, and Edgewood, and 9–13 % lower than OMI at Padonia and Essex. Inconsistent results at Fair Hill, with a high bias in the OMI retrievals (44 %) vs. Pandora and a low bias (6.7 %) vs. aircraft measurements, suggest differences in sampling area by the three independent measurement systems.

We also compare long-term observations of the total NO_2 columns by the OMI and Pandora instruments at the CAPABLE site. Figure 7 shows the multi-year monthly mean variation of OMI and Pandora NO_2 columns. NO_2 retrievals from the two instruments are moderately correlated ($r = 0.5$, $N = 163$), with the largest correlation ($r = 0.71$, $N = 40$) in winter and smallest correlation ($r = 0.25$, $N = 33$) in spring. However, the magnitude of the seasonal cycle differs for the two measurements, and they are not in phase. The seasonal variation in Pandora NO_2 columns exhibits a summer maximum and fall minimum, in contrast to the winter maximum and summer minimum in OMI total columns. The monthly mean biases range from −2.8 % in January to −28.4 % in June (Pandora being higher). The seasonal cycle in tropospheric and

ACPD
14, 14519–14573, 2014

stratospheric NO_2 columns retrieved from OMI and simulated from GMI are highly consistent (not shown), providing confidence in the seasonal variation in the OMI retrievals. Several factors could contribute to the observed seasonal biases between the OMI and Pandora retrievals. Due to the close proximity to local traffic at Langley Air Force Base, and the Yorktown power plant, Pandora measurements are influenced by local NO_x emission sources and could exhibit a dampened seasonal tropospheric NO_2 cycle. Also, unlike the OMI retrievals, the Pandora retrievals are based on the NO_2 cross-section at a constant temperature of 255 K (representing the stratosphere and troposphere), which could affect seasonal variation in the retrieved NO_2 columns. However, the effect of the temperature error in Pandora data is small (~ 3.3 % per 10° change in NO_2 temperature) and is unlikely to explain the observed seasonal differences. Errors in absolute calibration could lead to $\pm 2.7 \times 10^{15}$ molec. cm^{-2} uncertainty in Pandora NO_2 slant columns, with a similar uncertainty in vertical columns in summer, but only half of that in winter, favoring wintertime data, which are in excellent agreement with the OMI retrievals.

3.2.3 Comparison with MAX-DOAS measurements

Tropospheric NO_2 column retrievals from OMI are compared with long-term MAX-DOAS measurements at two Japanese sites, Tsukuba and Hedo, for the period 2006–2011. Figure 8 (left) compares tropospheric NO_2 columns retrieved from OMI and MAX-DOAS instruments. Tropospheric NO_2 columns over Hedo range over 0.2–3.2×10^{15} molec. cm^{-2} for MAX-DOAS and -0.5–2.8×10^{15} molec. cm^{-2} for OMI. The stratosphere–troposphere separation scheme in the OMI retrievals could yield slightly negative tropospheric columns in remote areas when measured slant columns are lower than estimated stratospheric slant columns. NO_2 columns over Tsukuba are much higher, reaching 40×10^{15} molec. cm^{-2} in both the MAX-DOAS and OMI data. Measurements from the two techniques exhibit a significant spatio-temporal correla-

ACPD
14, 14519–14573, 2014

tion (r = 0.86, N = 626). The mean relative difference between OMI and MAX-DOAS measurements is −16.3 % in Tsukuba and 7.1 % in Hedo.

Figure 8 (right) presents the seasonal mean tropospheric NO_2 column from MAX-DOAS measurements and those retrieved from OMI. The seasonal variation of the OMI-retrieved NO_2 columns is consistent with the MAX-DOAS measurements. The seasonal mean NO_2 columns for the MAX-DOAS measurements decrease by a factor of 1.6–1.9 from winter to summer, compared with a factor of 1.4–1.5 for OMI. The relative difference between OMI and MAX-DOAS seasonal mean tropospheric NO_2 columns range from 0.5 % in fall to −20.8 % in winter at Tsukuba and from −21.3 % in winter to 24.8 % in spring at Hedo. These results are generally consistent with the comparisons made with aircraft and Pandora observations.

3.2.4 Comparison with in situ surface measurements

We conduct an indirect validation of cloud-free (cloud radiance fraction < 0.5) OMI tropospheric NO_2 columns by comparison with coincident hourly in situ surface NO_2 measurements. This approach requires estimating ground-level NO_2 concentrations from OMI. We follow the method of Lamsal et al. (2008) with improvements as described in Lamsal et al. (2013) that combines coincidently sampled NO_2 vertical profile taken from a GEOS-Chem nested simulation (see Appendix B) with the OMI observations containing information about the spatial variation of the tropospheric NO_2 columns in the boundary layer. The OMI-derived surface NO_2 represents the mean mixing ratio in the lowest vertical layer (∼ 50 m) of the model.

We compare the OMI-derived surface NO_2 mixing ratios with the in situ measurements at the two rural surface sites, in Yorkville and Centerville for 2006–2010. Figure 9 displays the seasonal average surface NO_2 mixing ratios from the in situ measurements and those derived from the OMI retrievals. The OMI-derived surface NO_2 concentrations are well correlated with the photolytic converter measurements (r = 0.61, N = 700 for Yorkville and r = 0.69, N = 676 for Centerville) and exhibit similar seasonal variation with summertime minima. The OMI-derived surface NO_2 are lower than the in situ

ACPD
14, 14519–14573, 2014

measurements at Centerville by 11.8 % in fall but higher by 4.1 % in spring. Discrepancies are larger at Yorkville, where the OMI-derived surface NO_2 overestimates in situ measurements by 8.2 % in spring and underestimates by 25–31 % in other seasons.

3.2.5 Comparison with bottom-up emissions

We use an inventory of US NO_x emissions to indirectly validate OMI tropospheric NO_2 columns. We employ the emissions for 2005 as implemented in the GEOS-Chem model (Appendix B). Emissions employed by the GMI (Appendix A) simulation used in the operational retrieval included outdated North American NO_x emissions not suitable for validation. In GEOS-Chem, the bottom-up emissions over the US comprise over 75 % of NO_x emissions from anthropogenic activities; the remainder comes from soil, lightning, and biomass burning emissions. In contrast to inventories in developing countries, the US national emission inventory is more complete, accurate, and transparent (NARSTO, 2005), and is expected to be less uncertain (< 25 %, Christian Hogrefe, personal communication, 2008) at least in national totals. The largest contributors to the US NO_x emissions include on- and off-road vehicles (∼ 62 %) and electricity and industrial power generation (∼ 27 %), which exhibit little seasonal variation (EPA, 2009; Lamsal et al., 2010), a characteristic that is useful to assess seasonal variation in OMI retrievals. Difficulty could arise for comparisons focussed on county or sectoral levels, where uncertainty in bottom-up emissions could be significant, and in spring and summer, when emissions from soils and biomass burning are at peak levels.

To compare the OMI retrievals with NO_x emissions, we follow a simple mass balance approach (Martin et al., 2003; Lamsal et al., 2010), which directly relates OMI tropospheric NO_2 columns (Ω) to surface NO_x emissions (E):

$$E = \frac{E_M}{\Omega_M} \times \Omega. \quad (2)$$

Here, Ω_M is the tropospheric NO_2 column from a GEOS-Chem nested simulation based on the a priori surface NO_x emissions E_M, both sampled at the OMI overpass

ACPD
14, 14519–14573, 2014

time. To account for the impact of spatial smearing (Palmer et al., 2003), we considered an approach that accounts for the emissions from eight adjacent model grid cells to estimate surface NO_x emissions ($E_{i,j}$) at grid cell (i, j) from OMI (Toenges-Schüller et al., 2006; Boersma et al., 2008a; Lamsal et al., 2010) with improvements as discussed in Tang et al. (2013):

$$E_{i,j} = \frac{E'_{M_{i,j}}}{\sum_{n=-1}^{1}\sum_{m=-1}^{1} K_{i,j} E'_{M_{i+m,j+n}}} \times \frac{E_{M_{i,j}}}{\Omega_{M_{i,j}}} \times \Omega_{i,j}. \quad (3)$$

The smoothing kernel (K) is defined as $\frac{1}{p+8}\begin{bmatrix} 1 & 1 & 1 \\ 1 & p & 1 \\ 1 & 1 & 1 \end{bmatrix}$, where p is the smoothing parameter. To determine the value of p, we applied K to each grid cell in the bottom-up NO_x emission inventory with different p values, and computed the correlation between smoothed 24 h averaged bottom-up NO_x emissions ($E'_{i,j}$) and corresponding modeled tropospheric NO_2 columns. The maximum correlation coefficient corresponding to the optimal value of p was achieved at $p = 12$ as in Boersma et al. (2008a), which we adopt to infer monthly top-down surface NO_x emissions from OMI.

Figure 10 shows the spatial variation of bottom-up and OMI-based top-down NO_x inventories of land surface emissions. Both top-down and bottom-up inventories exhibit similarity in their spatial patterns, with large emissions in major urban centers, reflecting industrialization, dense traffic and population. The top-down and bottom-up annual surface NO_x emissions are strongly correlated ($r = 0.95$, $N = 2706$). The difference between the OMI-derived and bottom-up annual surface NO_x emissions integrated over the continental US is 8.8 %, much lower than the uncertainty in the bottom-up inventory and in the daily OMI retrievals. Excluding the smoothing parameter in the inversion, the difference decreases to 3.5 %. Despite excellent agreement in the total surface NO_x emissions, we observe a pronounced difference of up to a factor-of-two in the magnitude of local and regional NO_x emissions. These differences could arise from errors in the bottom-up emissions, in the OMI retrievals, and from the simple inversion scheme.

ACPD
14, 14519–14573, 2014

Figure 10 (bottom right) shows the ratio of the seasonal area-integrated OMI-derived and bottom-up NO_x emissions over the US. The ratio ranges from 0.91 in July to 1.35 in April. These results suggest consistency between bottom-up emissions and OMI retrievals within the range of their uncertainties.

3.2.6 Synthesis of validation results

Direct validation results of OMI NO_2 retrievals vs. in situ aircraft, MAX-DOAS, and ground direct sun Pandora measurements, and indirect validation results of OMI-derived surface NO_2 vs. in situ surface measurements and top-down vs. bottom-up emission inventories suggest the scientifically useful quality of the archived tropospheric NO_2 product from the standard OMI operational algorithm. Table 2 contains a summary of these validation results. OMI tropospheric NO_2 data generally correlate well ($r > 0.5$), agree to within ±20 % with biases tending to be more negative than positive, and exhibit similarity in monthly/seasonal variation with the independent data sets. These results are impressive considering the inherent limitations associated with the uncertainties in OMI retrievals and currently available validation data sets. Both temporal and spatial incoherence causes complications in comparing satellite observations with ground-based and aircraft measurements and can often result in misleading conclusions. NO_2 in the lower troposphere is short-lived and is concentrated close to emission sources. Ground-based and in situ instruments offer local measurements, in contrast to satellite observations averaged over a large field of view covering several hundred square kilometres. Therefore, differences between the two measurements ought to be expected simply due to NO_2 spatial inhomogeneity. The sampling differences can be reduced by acquiring long time series of NO_2 measurements, preferably in background locations with more homogeneous distributions.

Although OMI tropospheric NO_2 retrievals show promise and generally compare well with ground truth, occasional large differences could be due to errors in OMI tropospheric NO_2 columns. Principal sources of error in OMI tropospheric column density are radiometric errors, slant column density calculation, the air mass factor, the

ACPD
14, 14519–14573, 2014

retrieved cloud parameters, and the stratosphere–troposphere separation procedure. The tropospheric air mass factor is highly sensitive to errors in surface reflectivity in polluted areas with low surface reflectivity (e.g. Boersma et al., 2004). Further, the tropospheric air mass factor is calculated assuming the NO_2 retrieval implicitly accounts for aerosols through OMI-retrieved cloud fraction and surface reflectivity. However, algorithmic bias due to the presence of actual aerosols has not been studied. We quantify the impact of the a priori NO_2 profiles in tropospheric NO_2 retrievals in Sect. 4.

4 Effect of NO_2 profiles in NO_2 retrievals

In this section, we use aircraft in situ NO_2 measurements coincident with OMI observations during the DISCOVER-AQ campaign in Maryland to explore the sensitivity of the retrieved tropospheric columns to the a priori profiles.

Conversion of the slant column (Ω_s) retrieved from the satellite-measured reflectance spectrum y to vertical NO_2 column (Ω_v) requires an AMF (A):

$$\Omega_v = \frac{\Omega_s(y)}{A(x_a, b)}. \quad (4)$$

The AMF, a measure of the sensitivity of ln(y) to NO_2, depends on both the a priori NO_2 profile x_a and the forward model parameters b, which include the optical geometry and atmospheric and surface properties (surface albedo, cloud fraction, and cloud height). NO_2 is optically thin in the visible; this allows the calculation of AMF with a profile of altitude-dependent scattering weights (w) computed from a radiative transfer model and the a priori NO_2 profile shape:

$$A_{trop} = \frac{\sum_{surface}^{tropopause} w \times x_a}{\sum_{surface}^{tropopause} x_a}, \quad (5)$$

ACPD
14, 14519–14573, 2014

where x_a is the partial NO_2 column. The scattering weights include layer-specific correction factors to account for the temperature dependence of the NO_2 absorption cross-section. The summation extending from the surface to the tropopause provides tropospheric AMF (A_{trop}).

We use Eq. (5) to re-compute tropospheric AMF (A_{trop_ac}) using the measured NO_2 vertical profiles from aircraft and re-calculate tropospheric NO_2 column $\Omega_{v,\,trop\_ac}$ from OMI tropospheric slant columns ($\Omega_{s,\,trop}$):

$$\Omega_{v,\,trop\_ac} = \frac{\Omega_{s,\,trop}}{A_{trop\_ac}} = \frac{\Omega_s - \Omega_{s,\,strat}}{A_{trop\_ac}}. \quad (6)$$

Here, Ω_s is the de-striped NO_2 slant column density (measured NO_2 slant column corrected for instrumental artifacts). The stratospheric slant columns ($\Omega_{s,\,strat}$) are calculated from the stratospheric NO_2 vertical columns and the stratospheric AMF, both available in the operational data product.

Figures 4 and 5 contain tropospheric NO_2 columns re-calculated with aircraft-mesured NO_2 vertical profiles. The OMI NO_2 retrievals calculated using the aircraft measured profiles differ from the operational retrievals calculated with model-simulated profiles by up to −43 %, much larger than previously reported (e.g. Boersma et al., 2004). Compared to the operational retrievals, the new retrievals are systematically lower by 16–19 % in rural locations and higher by 15–21 % in urban locations. These results are consistent with the previous study by Hains et al. (2010), who evaluated the impact of a priori profiles in the Dutch NO_2 (DOMINO) retrievals using observations from the Dutch Aerosol and Nitrogen Dioxide Experiments for vaLIdation of OMI and SCIAMACHY (DANDELIONS) and Intercontinental Chemical Transport Experiment Phase B (INTEX-B) campaigns. Our use of measured profiles improved the correlation between OMI and aircraft measurements over all locations and resulted in a significant correlation at Padonia ($r = 0.66$, $N = 9$) and Edgewood ($r = 0.75$, $N = 8$). Overall, the agreement between OMI and aircraft measurements improved in urban locations by 12–14 % and worsened at Aldino and Fair Hill by a similar magnitude.

ACPD
14, 14519–14573, 2014

Comparison of the OMI NO_2 retrievals calculated using the aircraft measured profiles with Pandora observations are presented in Figures 5 and 6. Except for Fair Hill, the correlation of OMI with Pandora improved with the new retrievals. The bias of the OMI retrievals against Pandora reduced at Fair Hill, Beltsville, and Edgewood, but increased at Aldino, Padonia, and Essex.

5 Application of OMI to evaluate AQ models

Several studies (e.g. van Noije et al., 2006; Lamsal et al., 2010) have compared model-simulated NO_2 columns with satellite retrievals. Such comparisons require coincident sampling of model output with observations, because inconsistent sampling could lead to significant differences and incorrect interpretation of the data. The most common approach to comparison involves examining and interpreting the difference between satellite observations and model results. This approach of direct comparison is expected to have difficulty when interpreting differences unless the a priori NO_2 vertical profile shapes used in the retrievals are from the model in question.

The operational NO_2 retrieval algorithm uses NO_2 shape factors generated from GMI simulation results, available at the resolution of $2^\circ \times 2.5^\circ$. The coarse-resolution model profiles may not sufficiently capture the actual vertical distribution of NO_2, especially where the horizontal gradient is large. Moreover, over the last decade, anthropogenic emissions of NO_x have undergone rapid changes that may change the local NO_2 shape factor and subsequently affect the retrieval of tropospheric NO_2. Use of profiles obtained from a model simulation performed with updated emissions at high resolution not only lead to more accurate retrievals through improved spatial representation of NO_2 shape factors in the AMF calculation, but it also ensures self-consistency when the OMI retrievals are compared with modeled NO_2 columns (Eskes and Boersma, 2003; Boersma et al., 2004).

Here, we show an example by comparing OMI tropospheric NO_2 retrievals with a model simulation. We consider the GEOS-Chem nested model (Appendix B) for

ACPD
14, 14519–14573, 2014

North America that includes updated emissions and performs simulation at high resolution 0.5° × 0.667°. As compared to the coarse model simulation, the fine model simulation can provide better representation of the vertical distributions of NO_2 in OMI pixels by considering changes in the NO_2 shape factors related to the changes in NO_x emissions. We use Eq. (5) to re-compute the tropospheric AMF (A_{trop_GC}) using the new profile and use Eq. (6) to re-calculate the tropospheric NO_2 column (OMI_GC) from OMI. For comparison, we use OMI pixels with cloud radiance fraction < 0.5 and surface reflectivity < 0.3 and calculate area-weighted average columns (Level 3) on a 0.5° × 0.667° grid.

Figure 11 shows seasonal mean tropospheric NO_2 columns from OMI and GEOS-Chem for 2005. Both show large NO_2 columns in dense urban areas in eastern North America and major metropolitan areas such as Los Angeles, San Francisco, Denver, and Houston. They exhibit a similar seasonal pattern, with a winter maximum, reflecting longer NO_x lifetime and shallower mixing layer depth in winter. The correlation between the GEOS-Chem model and OMI seasonal NO_2 columns is remarkable (r = 0.85–0.92). The seasonal average GEOS-Chem column is lower than the OMI column by 7 % in spring and higher by 24 % in summer yet within the estimated uncertainty of OMI retrievals and GEOS-Chem simulation.

OMI tropospheric NO_2 columns exhibit a number of differences with the modeled NO_2 columns (Fig. 11, fourth row). The modeled NO_2 columns are generally larger in some urban areas of the west coast and northeastern US and over the Canadian oil sands. Simulation from GEOS-Chem also indicates about factor-of-two higher columns in summer in the Midwest US, a major region of soil NO_x emissions. Retrieved columns are higher over the eastern US in spring, eastern Canada in winter, and cleaner background areas in all seasons. Some of these differences could point to certain emission sources that are not well represented in the model. Other sources of model bias include the errors in simulating OH concentrations, N_2O_5 hydrolysis rates, and vertical mixing that affect simulation of NO_x chemistry (van Noije et al., 2006; Valin et al., 2011).

ACPD
14, 14519–14573, 2014

Possible errors in OMI retrievals causing the observed difference cannot be ruled out. Due to several error sources in the AMF calculation, systematic biases in the spatial variation of OMI retrievals are expected. The spatial resolution of surface reflectivity and a priori NO_2 shape factor are coarser than the ground resolution of OMI, yielding errors in AMF. A change in surface reflectivity from 0.01 to 0.1 could alter the AMF by up to 90 % (Leitão et al., 2010), which suggests the importance of accurate knowledge of surface properties (McLinden et al., 2014) and potential impact of residual cloud contamination in the climatology of surface reflectivity. Lack of explicit treatment of aerosols in the AMF calculation could have a significant impact in the retrieval of tropospheric NO_2, although the effect could be moderate (7 %) over highly polluted areas (Leitão et al., 2010). Errors in retrievals could be quite large in cases of elevated aerosols in downwind areas, if those elevated aerosols are not accounted for.

Figure 11 (fifth row) shows the seasonal mean difference resulting from the use of GMI profile shapes in the AMF calculation. Since the GMI model and GEOS-Chem both use GEOS-5 meteorological fields and have similar tropospheric chemical mechanisms, the difference between the two retrievals is primarily due to differences in emissions. The anthropogenic emissions in the GMI simulation are appropriate for 1999, which is considerably higher than 2005 emissions over nearly all of North America, with the notable exception of the Alberta oil sands, where it is considerably lower. Resulting changes in local NO_2 profile shape impact tropospheric AMFs and, therefore, change individual retrievals by up to 40 % and seasonal averages by 1 % in winter and 12 % in fall.

6 Conclusions

We compared the OMI tropospheric NO_2 product (OMNO2, version 2.1) to ground-based measurements to assess the data quality, and to aircraft-based measurements, both to compare the retrieved column amounts and to assess the sensitivity of OMI NO_2 to the a priori profiles used in the retrieval. Model profiles were used to estimate

ACPD
14, 14519–14573, 2014

tropospheric column amounts from in situ measurements of NO_2 at ground-level. Finally, we investigated the potential improvement of the retrievals that could be realized using a higher-resolution model, with updated emissions inputs, as a source of a priori profiles. Table 2 summarizes the results of these investigations.

We examined NO_2 profiles measured in situ by the NCAR chemiluminescence instrument flown in the P-3B aircraft during the DISCOVER-AQ field campaign in the Baltimore-Washington, D.C. metropolitan region in July 2011. The P-3B aircraft provided NO_2 measurements from ~ 300 m in the boundary layer to ~ 3.3 km in the free-troposphere, allowing evaluation of tropospheric NO_2 from OMI and estimation of retrieval errors due to a priori NO_2 profiles from the Global Modeling Initiative model. The mean relative vertical distribution of NO_2 from aircraft and that calculated with the GMI model are in agreement to within 30 %, but observations also reveal a significant (up to a factor of two) day-to-day variability in NO_2 profile shape. Using aircraft NO_2 profiles altered tropospheric AMFs by up to 43 % on some days and yielded improved daily NO_2 column retrievals. Coincident OMI and aircraft measurements agree to within 20 % for a majority of cases, with low biases in OMI retrievals by 5.8–22.1 % at rural and urban locations and by 50 % in the coastal towns of Essex and Edgewood. Comparison of total NO_2 column measurements from OMI and Pandora instruments at those locations presented inconsistent results, suggesting low biases in OMI retrievals of < 6 % at Aldino, Beltsville, and Edgewood, and high biases of 9–13 % at Padonia and Essex. Spatial inhomogeneity within a satellite ground pixel, stratosphere–troposphere separation in OMI data, and differences in the sampling domain among the three measurements make short-term comparisons difficult.

We used ground-based data for an extended period of time to examine the seasonal variation of tropospheric NO_2 retrievals. Comparison with the MAX-DOAS measurements at a remote location in Hedo and an urban site in Tsukuba in Japan during 2006–2011 suggests that OMI and MAX-DOAS data are highly consistent ($r = 0.86$), with seasonal biases < 25 % and a mean bias of −16.3 % at Tsukuba and 7.1 % at Hedo in the OMI retrievals. The inconsistent seasonal variation in total NO_2 columns

ACPD
14, 14519–14573, 2014

from OMI and Pandora at Hampton, VA, likely arises from the influence of local NO_x emission sources in the Pandora measurements.

As an indirect validation, we derived the ground-level NO_2 from OMI using coincident GEOS-Chem NO_2 profiles and compared them with surface NO_2 measurements at two rural sites (Centerville, AL and Yorkville, GA) of the SEARCH network. The mean seasonal difference between the OMI-derived surface NO_2 and surface measurements ranges from −11.8 % (fall) to 4.1 % (spring) in Centerville and from −31 % (winter) to 8.2 % (spring) in Yorkville. Use of well-established seasonal bottom-up surface NO_x emissions inventories over the United States suggested that the monthly mean biases in OMI-derived top-down surface NO_x emissions range from −9 % in July to 35 % in April.

Overall, despite the typical complexities associated with the validation of satellite retrievals, OMI tropospheric NO_2 columns are consistent with and agree within the uncertainty of the validation datasets. Therefore, the OMI data offer the means to evaluate the fidelity of CTM model results. The comparison of model-simulated NO_2 columns with satellite retrievals should utilize scattering weights (or averaging kernels) that are made available with the OMI data files, to correct for the effect of climatological monthly a priori NO_2 profiles used in the retrievals. OMI retrieval algorithms could benefit from high-resolution surface reflectivity information and a priori NO_2 profiles and from the explicit treatment of aerosols. A coordinated effort in generating validation datasets by including remotely sensed and in situ observations at the ground, with balloon sondes, and from aircraft over a wide geographic region for a long time period will be valuable for assessing satellite retrievals.

Appendix A: GMI model description

Retrieval of tropospheric NO_2 columns from a satellite instrument requires an assumed vertical distribution of NO_2. Because NO_2 in situ profile measurements are very few, and because the spatial variability in NO_2 profiles is quite large, this is best achieved

ACPD
14, 14519–14573, 2014

from a global three-dimensional chemical transport model for atmospheric composition. We use the Global Modeling Initiative (GMI) model (Strahan et al., 2007), consisting of a chemical mechanism that combines the stratospheric mechanism described in Douglass et al. (2004) with a version of the tropospheric mechanism in GEOS-Chem (Bey et al., 2001) with modifications as described in Duncan et al. (2007). The model is driven by assimilated meteorological fields from the Goddard Earth Observing System (GEOS) at the NASA Global Modeling and Assimilation Office (GMAO, http://gmao.gsfc.nasa.gov/). The GEOS-5 meteorological data are provided every 3–6 h (3 h for surface fields and mixing depths) at 72 pressure levels in the vertical, extending from surface to 0.01 hPa.

The model includes the global anthropogenic emissions from the Global Emission Inventory Activity [GEIA, (Benkovitz et al., 1996) for the base year of 1985 and scaled to 1995, as described in Bey et al. (2001). The global inventory is replaced by the following regional inventories: the US EPA National Emissions Inventory (NEI) for 1999 over the United States, the Criteria Air Contaminants (CAC) inventory (http://www.ec.gc.ca/inrp-npri) for 2000 over Canada, the Big Bend Regional Aerosol and Visibility Observational Study (BRAVO) inventory for 1999 over Mexico (Kuhns et al., 2005), the European Monitoring and Evaluation Programme (EMEP) inventory for 2000 over Europe, and the inventory from Streets et al. (2006) for 2006 over East Asia. The GMI model also includes NO_x emissions from soil, lightning, biomass burning, biofuel, and aircraft sources, as described in Duncan et al. (2007).

In this work, the model simulation was conducted at the resolution of $2^{\circ} \times 2.5^{\circ}$ for three years (2005–2007). Model outputs were sampled at the local time of OMI overpass. Since monthly mean values capture the seasonal variation, we derived monthly mean values for NO_2 and temperature profiles and tropopause pressures needed for the calculation of the AMF.

ACPD
14, 14519–14573, 2014

Appendix B: GEOS-Chem model description

We use the GEOS-Chem three-dimensional model of tropospheric chemistry (Bey et al., 2001), version 9-01-03 (www.geos-chem.org), to demonstrate the application of scattering weights to re-calculate the OMI tropospheric NO_2 column and to examine the effect of NO_2 profile shape in retrievals of tropospheric NO_2 columns. We employ GEOS-Chem nested simulations (Zhang et al., 2011; Wang et al., 2012; van Donkelaar et al., 2012; Lamsal et al., 2013) with a horizontal grid size of $\frac{1}{2}^\circ \times \frac{2}{3}^\circ$ over North America (10–70° N, 40–140° W). Boundary conditions of the nested region are provided by the global simulation at $2^\circ \times 2.5^\circ$. The GEOS-Chem simulation is driven by assimilated meteorological data available from the Goddard Earth Observing System GEOS-5 at the NASA GMAO. The model includes a detailed simulation of tropospheric ozone-NO_x-hydrocarbon chemistry as well as of aerosols and their precursors (Bey et al., 2001; Park et al., 2004).

The global anthropogenic emissions in this GEOS-Chem simulation are from EDGAR 3.2FT2000 (Olivier et al., 2001) for 2000, which are scaled to 2005 following van Donkelaar et al. (2008). The global inventory is overwritten by the following regional inventories: The US EPA NEI for 2005 over the United States, the CAC inventory (http://www.ec.gc.ca/inrp-npri) for 2005 over Canada, the BRAVO inventory (Kuhns et al., 2005) for 1999 over Mexico, the EMEP inventory for 2005 over Europe, the inventory from Zhang et al. (2007) for 2006 over East Asia. NO_x emissions from soils, lightning, biomass burning, and aircraft are as described in Lamsal et al. (2010, 2011).

The GEOS-Chem simulation of NO_x has been evaluated extensively with in situ and satellite observations and generally agrees to within 30 % of measured NO_x (Martin et al., 2006; Hudman et al., 2007; Boersma et al., 2008b). We conducted a simulation for the year 2005 and sample the model output between 13:00 and 15:00 local time for analysis of the OMI data.

ACPD
14, 14519–14573, 2014

Acknowledgements. The work was supported by NASA's Earth Science Division through an Aura Science team grant. The Dutch-Finnish-built OMI instrument is part of the NASA EOS Aura satellite payload. The OMI instrument is managed by KNMI and the Netherlands Agency for Aero-space Programs (NIVR).

References

Bechle, M. J., Millet, D. B., and Marshall, J. D.: Remote sensing of exposure to NO_2, satellite versus ground-based measurement in a large urban, Atmos. Environ., 69, 345–353, doi:10.1016/j.atmosenv.2012.11.046, 2013. 14522

Beirle, S., Platt, U., Wenig, M., and Wagner, T.: Weekly cycle of NO_2 by GOME measurements: a signature of anthropogenic sources, Atmos. Chem. Phys., 3, 2225–2232, doi:10.5194/acp-3-2225-2003, 2003. 14522

Beirle, S., Boersma, K. F., Platt, U., Lawrence, M. G., and Wagner, T.: Megacity emissions and lifetimes of nitrogen oxides probed from space, Science, 333, 1737–1739, doi:10.1126/science.1207824, 2011. 14522

Benkovitz, C. M., Scholtz, M. T., Pacyna, J., Terrasón, L., Dignon, J., Voldner, E. C., Spiro, P. A., Logan, J. A., and Graedel, T. E.: Global gridded inventories of anthropogenic emissions of sulfur and nitrogen, J. Geophys. Res., 101, 29239–29253, 1996. 14546

Bey, I., Jacob, D. J., Yantosca, R. M., Logan, J. A., Field, B. D., Fiore, A. M., Li, Q., Liu, H. Y., Mickley, L. R., and Schultz, M. G.: Global modeling of tropospheric chemistry with assimilated meteorology: model description and evaluation, J. Geophys. Res., 106, 23073–23096, 2001. 14546, 14547

Blond, N., Boersma, K. F., Eskes, H. J., van der A, R. J., Van Roozendael, M., De Smedt, I., Bergametti, G., and Vautard, R.: Intercomparison of SCIAMAHCY nitrogen dioxide observations, in situ measurements and air quality modeling results over Western Europe, J. Geophys. Res., 112, D10311, doi:10.1029/2006JD007277, 2007. 14523

Boersma, K. F., Eskes, H. J., and Brinksma, E. J.: Error analysis for tropospheric NO_2 retrieval from space, J. Geophys. Res., 109, D04311, doi:10.1029/2003JD003962, 2004. 14525, 14539, 14540, 14541

Boersma, K. F., Eskes, H. J., Veefkind, J. P., Brinksma, E. J., van der A, R. J., Sneep, M., van den Oord, G. H. J., Levelt, P. F., Stammes, P., Gleason, J. F., and Bucsela, E. J.:

ACPD
14, 14519–14573, 2014

Near-real time retrieval of tropospheric NO_2 from OMI, Atmos. Chem. Phys., 7, 2103–2118, doi:10.5194/acp-7-2103-2007, 2007. 14525

Boersma, K. F., Jacob, D. J., Bucsela, E. J., Perring, A. E., Dirksen, R., van der A, R. J., Yontosca, R. M., Park, R. J., Wenig, M. O., Bertram, T. H., and Cohen, R. C.: Validation of OMI tropospheric NO_2 observations during INTEX-B and application to constrain NO_x emissions over the eastern United States and Mexico, Atmos. Environ., 42, 4480–4497, 2008a. 14522, 14537

Boersma, K. F., Jacob, D. J., Eskes, H. J., Pinder, R. W., Wang, J., and van der A, R. J.: Intercomparison of SCIAMACHY and OMI tropospheric NO_2 columns: observing the diurnal evolution of chemistry and emissions from space, J. Geophys. Res., 113, D16S26, doi:10.1029/2007JD008816, 2008b. 14547

Boersma, K. F., Jacob, D. J., Trainic, M., Rudich, Y., DeSmedt, I., Dirksen, R., and Eskes, H. J.: Validation of urban NO_2 concentrations and their diurnal and seasonal variations observed from the SCIAMACHY and OMI sensors using in situ surface measurements in Israeli cities, Atmos. Chem. Phys., 9, 3867–3879, doi:10.5194/acp-9-3867-2009, 2009. 14523

Boersma, K. F., Eskes, H. J., Dirksen, R. J., van der A, R. J., Veefkind, J. P., Stammes, P., Huijnen, V., Kleipool, Q. L., Sneep, M., Claas, J., Leitão, J., Richter, A., Zhou, Y., and Brunner, D.: An improved tropospheric NO_2 column retrieval algorithm for the Ozone Monitoring Instrument, Atmos. Meas. Tech., 4, 1905–1928, doi:10.5194/amt-4-1905-2011, 2011. 14525

Brinksma, E., Pinardi, G., Braak, R., Volten, H., Richter, A., Schonhardt, A., Van Roozendael, M., Fayt, C., Hermans, C., Dirksen, R., Vlemmix, T., Berkhout, A. J. C., Swart, D. P. J., Oetjen, H., Wittrock, F., Wagner, T., Ibrahim, O. W., de Leeuw, G., Moerman, M., Curier, R. L., Celarier, E. A., Knap, W. H., Veefkind, J. P., Eskes, H. J., Allaart, M., Rothe, R., Piters, A. J. M., and Levelt, P.: The 2005 and 2006 DANDELIONS NO_2 and aerosol intercomparison campaigns, J. Geophys. Res., 113, D16S46, doi:10.1029/2007JD008808, 2008. 14522

Bucsela, E. J., Celarier, E. A., Wenig, M. O., Gleason, J. F., Veefkind, J. P., Boersma, K. F., and Brinksma, E. J.: Algorithm for NO_2 vertical column retrieval from the ozone monitoring instrument, IEEE Trans. Geosci. Remote, 44, 1245–1258, 2006. 14525

Bucsela, E. J., Perring, A. E., Cohen, R. C., Boersma, K. F., Celarier, E. J., Gleason, J. F., Wenig, M. O., Bertram, T. H., Wooldrige, P. J., Dirksen, R., and Veefkind, J. P.: Comparison of NO_2 in situ aircraft measurements with data from the ozone monitoring instrument, J. Geophys. Res., 113, D16S31, doi:10.1029/2007JD008838, 2008. 14522, 14523

ACPD
14, 14519–14573, 2014

Bucsela, E. J., Pickering, K. E., Huntermann, T. L., Cohen, R. C., Perring, A., Gleason, J. F., Blakeslee, R. J., Albrecht, R. I., Holzworth, R., Cipriani, J. P., Vargas-Navarro, D., Mora-Segura, I., Pacheco-Hernández, A., and Laporte-Molina, A.: Lightning-generated NO_x seen by the Ozone monitoring instrument during NASA'S Tropical Composition, Cloud and Climate Coupling experiment (TC4), J. Geophys. Res., 115, D00J10, doi:10.1029/2009JD013118, 2010. 14522

Bucsela, E. J., Krotkov, N. A., Celarier, E. A., Lamsal, L. N., Swartz, W. H., Bhartia, P. K., Boersma, K. F., Veefkind, J. P., Gleason, J. F., and Pickering, K. E.: A new stratospheric and tropospheric NO_2 retrieval algorithm for nadir-viewing satellite instruments: applications to OMI, Atmos. Meas. Tech., 6, 2607–2626, doi:10.5194/amt-6-2607-2013, 2013. 14522, 14525, 14526

Cede, A., Herman, J., Richter, A., Krotkov, N. A., and Burrows, J. P.: Measurements of nitrogen dioxide total column amounts using a Brewer double spectrophotometer in direct sun mode, J. Geophys. Res., 111, D05304, doi:10.1029/2005JD006585, 2006. 14529

Celarier, E. A., Brinksma, E. J., Gleason, J. F., Veefkind, J. P., Cede, A., Herman, J. R., Ionov, D., Goutail, F., Pommereau, J. P., Lambert, J. C., van Roozendael, M., Pinardi, G., Witrrock, F., Schönhardt, A., Richter, A., Ibrahim, O. W., Wagner, T., Bojkov, B., Mount, G., Spinei, E., Chen, C. M., Pongetti, T. J., Sander, S. P., Bucsela, E. J., Wenig, M. O., Swart, D. P. J., Volten, H., Kroon, M., and Levelt, P. F.: Validation of ozone monitoring instrument nitrogen dioxide columns, J. Geophys. Res., 113, D15S15, doi:10.1029/2007JD008908, 2008. 14522

Crawford, J., Pickering, K. E. et al: DISCOVER-AQ Overview, TBD, http://www-air.larc.nasa.gov/missions/discover-aq/discover-aq.html, 2014. 14526

de Wildt, M. R., Eskes, H., and Boersma, K. F.: The global economic cycle and satellite-derived NO_2 trends over shipping lanes, Geophys. Res. Lett., 39, l01802, doi:10.1029/2011GL049541, 2012. 14522

Dobber, M. R., Kleipool, Q., Dirksen, R., Levelt, P. F., Jaross, G., Taylor, S., Kelly, T., Flynn, L., Leppelmeier, G., and Rozemeijer, N.: Validation of ozone monitoring instrument level 1b data products, J. Geophys. Res., 113, D15S06, doi:10.1029/2007JD008665, 2008. 14525, 14526

Douglass, A. R., Stolarski, R. S., Strahan, S. E., and Connell, P. S.: Radicals and reservoirs in the GMI chemistry and transport model: comparison to measurements, J. Geophys. Res., 109, D16302, doi:10.1029/2004JD004632, 2004. 14546

ACPD
14, 14519–14573, 2014

Duncan, B. N., Strahan, S. E., Yoshida, Y., Steenrod, S. D., and Livesey, N.: Model study of the cross-tropopause transport of biomass burning pollution, Atmos. Chem. Phys., 7, 3713–3736, doi:10.5194/acp-7-3713-2007, 2007. 14546

Duncan, B. N., Yoshida, Y., de Foy, B., Lamsal, L. N., Streets, D., Lu, Z., Pickering, K. E., and Krotkov, N. A.: The observed response of the ozone monitoring instrument (OMI) NO_2 column to NO_x emission controls on power plants in the United States: 2005–2011, Atmos. Environ., 81, 102–111, 2013. 14522

Edgerton, E. S., Hartsell, B. E., Saylor, R. D., Jansen, J. J., Hansen, D. A., and Hidy, G. M.: The southeastern aerosol research and characterization study, part 3: Continuous measurements of fine particulate matter mass and composition, J. Air Waste Manage. Assoc., 56, 1325–1341, 2006. 14530

EPA: Primary national ambient air quality standard for nitrogen dioxide, Tech. rep., Environmental Protection Agency, Federal Register, Washington DC 20460, Vol. 74, No. 134, 2009. 14522, 14536

Eskes, H. J. and Boersma, K. F.: Averaging kernels for DOAS total-column satellite retrievals, Atmos. Chem. Phys., 3, 1285–1291, doi:10.5194/acp-3-1285-2003, 2003. 14541

Flynn, C. M., Pickering, K. E., Crawford, J. H., Lamsal, L. N., Krotkov, N. A., Herman, J., Weinheimer, A., Chen, G., Liu, X., Szykman, J., Tsay, S. C., Laughner, C. P., Hains, J., Lee, P., Dickerson, R. R., Stehr, J. W., and Brent, L.: The relationship between column-density and surface mixing ratio: statistical analysis of O_3 and NO_2 data from the July 2011 Maryland DISCOVER-AQ mission, Atmos. Environ., 92, 429–441, 2014.

Ghude, S. D., Lal, D. M., Beig, G., van der A, R., and Sable, D.: Rain-induced soil NO_x emission from India during the onset of the summer monsoon: a satellite perspective, J. Geophys. Res., 115, D16304, doi:10.1029/2009JD013367, 2010. 14522

Ghude, S. D., Pfister, G. G., Jena, C., van der A, R., Emmons, L. K., and Kumar, R.: Satellite constraints of nitrogen oxide emissions from India based on OMI observations and WRF-Chem simulations, Geophys. Res. Lett., 40, 1–6, doi:10.1029/2012GL053926, 2013a. 14522

Ghude, S. D., Kulkarni, S. H., Jena, C., Pfister, G. G., Beig, G., Fadnavis, S., and van der A, R. J.: Application of satellite observations for identifying regions of dominant sources of nitrogen oxides over the Indian Subcontinent, J. Geophys. Res., 118, 1075–1089, doi:10.1029/2012JD017811, 2013b. 14522

Hains, J., Boersma, K. F., Kroon, M., Dirksen, R. J., Cohen, R. C., Perring, A. E., Bucsela, E., Volten, H., Swart, D. P. J., Richter, A., Wittrock, F., Schoenhardt, A., Wagner, T.,

ACPD
14, 14519–14573, 2014

Ibrahim, O.W., van Roozendael, M., Pinardi, G., Gleason, J. F., Veefkind, J. P., and Levelt, P.: Testing and improving OMI DOMINO tropospheric NO_2 using observations from the DANDELIONS and INTEX-B validation campaigns, J. Geophys. Res., 115, D05301, doi:10.1029/2009JD012399, 2010. 14522, 14540

Heland, J., Schlager, H., Richter, A., and Burrows, J. P.: First comparison of tropospheric NO_2 column densities retrieved from GOME measurements and in situ aircraft profile measurements, Geophys. Res. Lett., 29, 1983, doi:10.1029/2002GL015528, 2002. 14522

Herman, J. R., Cede, A., Spinei, E., Mount, G., Tzortziou, M., and Abuhassan, N.: NO_2 column amounts from ground-based Pandora and MFDOAS spectrometers using the direct-sun DOAS technique: intercomparisons and application to OMI validation, J. Geophys. Res., 114, D13307, doi:10.1029/2009JD011848, 2009. 14529, 14530, 14532

Herron-Thorpe, F. L., Lamb, B. K., Mount, G. H., and Vaughan, J. K.: Evaluation of a regional air quality forecast model for tropospheric NO_2 columns using the OMI/Aura satellite tropospheric NO_2 product, Atmos. Chem. Phys., 10, 8839–8854, doi:10.5194/acp-10-8839-2010, 2010. 14522

Hilboll, A., Richter, A., and Burrows, J. P.: Long-term changes of tropospheric NO_2 over megacities derived from multiple satellite instruments, Atmos. Chem. Phys., 13, 4145–4169, doi:10.5194/acp-13-4145-2013, 2013. 14522

Hirsch, R. M. and Gilroy, E. J.: Methods of fitting a straight line to data: examples in water resources, Water Res. Bull., 20, 705–711, 1984. 14570

Hönninger, G., von Friedeburg, C., and Platt, U.: Multi axis differential optical absorption spectroscopy (MAX-DOAS), Atmos. Chem. Phys., 4, 231–254, doi:10.5194/acp-4-231-2004, 2004. 14528

Hudman, R. C., Jacob, D. J., Turquety, S., Leibensperger, E. M., Murray, L. T., Wu, S., Gilliland, A. B., Avery, M., Bertram, T. H., Brune, W., Cohen, R. C., Dibb, J. E., Flocke, F. M., Fried, A., Holloway, J., Neuman, J. A., Orville, R., Perring, A., Ren, X., Sachse, G. W., Singh, H. B., Swanson, A., and Wooldridge, P. J.: Surface and lightning sources of nitrogen oxides over the United States: magnitudes, chemical evolution, and outflow, J. Geophys. Res., 112, doi:10.1029/2006JD007912, 2007. 14547

Huijnen, V., Eskes, H. J., Poupkou, A., Elbern, H., Boersma, K. F., Foret, G., Sofiev, M., Valdebenito, A., Flemming, J., Stein, O., Gross, A., Robertson, L., D'Isidoro, M., Kioutsioukis, I., Friese, E., Amstrup, B., Bergstrom, R., Strunk, A., Vira, J., Zyryanov, D., Maurizi, A., Melas, D., Peuch, V.-H., and Zerefos, C.: Comparison of OMI NO_2 tropospheric

ACPD
14, 14519–14573, 2014

columns with an ensemble of global and European regional air quality models, Atmos. Chem. Phys., 10, 3273–3296, doi:10.5194/acp-10-3273-2010, 2010. 14522

Intergovernmental Panel on Climate Change (IPCC): Contribution of working group I to the Fourth Assessment Report of the Intergovernmental Panel on Climate Change, in: Climate Change 2007: The Physical Science Basis, edited by: Solomon, Qin, S., Manning, M., Chen, Z., Marquis, M., Averyt, K. B., Tignor, M., and Miller, H. L., 996 pp., Cambridge University Press, Cambridge, UK, 2007. 14521

Ionov, D. V., Timofeyev, Y. M., Sinyakov, V. P., Semenov, V. K., Goutail, F., Pommereau, J. P., Bucsela, E. J., Celarier, E. A., and Kroon, M.: Ground-based validation of EOS-Aura OMI NO_2 vertical column data in the midlatitude mountain ranges of Tien Shan (Kyrgyzstan) and Alps (France), J. Geophys. Res., 113, 4437, doi:10.1029/2007JD008659, 2008. 14522

Irie, H., Kanaya, Y., Akimoto, H., Tanimoto, H., Wang, Z., Gleason, J. F., and Bucsela, E. J.: Validation of OMI tropospheric NO_2 column data using MAX-DOAS measurements deep inside the North China Plain in June 2006: Mount Tai Experiment 2006, Atmos. Chem. Phys., 8, 6577–6586, doi:10.5194/acp-8-6577-2008, 2008. 14522, 14529

Irie, H., Boersma, K. F., Kanaya, Y., Takashima, H., Pan, X., and Wang, Z. F.: Quantitative bias estimates for tropospheric NO_2 columns retrieved from SCIAMACHY, OMI, and GOME-2 using a common standard for East Asia, Atmos. Meas. Tech., 5, 2403–2411, doi:10.5194/amt-5-2403-2012, 2012. 14523, 14528, 14529

Jaeglé, L., Steinberger, L., Martin, R. V., and Chance, K.: Global partitioning of NO_x sources using satellite observations: Relative roles of fossil fuel combustion, biomass burning and soil emissions, Faraday Discuss., 130, 4537, doi:10.1039/b502128f, 2005. 14522

Kim, S. W., Heckel, A., McKeen, S. A., Frost, G. J., Hsie, E. Y., Trainer, M. K., Richter, A., Burrows, J. P., Peckham, S. E., and Grell, G. A.: Satellite-observed US power plant NO_x emission reductions and their impact on air quality, Geophys. Res. Lett., 33, L22812, doi:10.1029/2006GL027749, 2006. 14522

Kim, S. W., Heckel, A., Frost, G. J., Richter, A., Gleason, J., Burrows, J. P., McKeen, S. A., Hsie, E. Y., Granier, C., and Trainer, M. K.: NO_2 columns in the western United States observed from space and simulated by a regional chemistry model and their implications for NO_x emissions, J. Geophys. Res., 114, D11301, doi:10.1029/2008JD011343, 2009. 14522

Knepp, T., Pippin, M., Crawford, J., Chen, G., Szykman, J., Long, R., Cowen, L., Cede, A., Abuhassan, N., Herman, J., Delgado, R., Compton, J., Berkoff, T., Fishman, J., Martins, D., Stauffer, R., Thompson, A. M., Weinheimer, A., Knapp, D., Montzka, D., Lenschow, D., and

ACPD
14, 14519–14573, 2014

Neil, D.: Estimating surface NO_2 and SO_2 mixing ratios from fast-response total column observations and potential application to geostationary missions, J. Atmos. Chem., D15308, doi:10.1007/s10874-013-9257-6, 2013. 14529

Konovalov, I. B., Beekmann, M., Richter, A., and Burrows, J. P.: Inverse modelling of the spatial distribution of NO_x emissions on a continental scale using satellite data, Atmos. Chem. Phys., 6, 1747–1770, doi:10.5194/acp-6-1747-2006, 2006. 14522

Kramer, L. J., Leigh, R. J., Remedios, J. J., and Monks, P. S.: Comparison of OMI and ground-based in situ and MAX-DOAS measurements of tropospheric nitrogen dioxide in an urban area, J. Geophys. Res., 113, D16S39, doi:10.1029/2007JD009168, 2008. 14522

Kuhns, H., Knipping, E. M., and Vokovich, J. M.: Development of a United States-Mexico emissions inventory for the Big Bend Regional Aerosol and Visibility Observational (BRAVO) study, J. Air Waste Mgt. Assoc., 55, 677–692, 2005. 14546, 14547

Lamsal, L. N., Martin, R. V., van Donkelaar, A., Steinbacher, M., Celarier, E. A., Bucsela, E., Dunlea, E. J., and Pinto, J. P.: Ground-level nitrogen dioxide concentrations inferred from the satellite-borne ozone monitoring instrument, J. Geophys. Res., 113, D16308, doi:10.1029/2007JD009235, 2008. 14522, 14523, 14535

Lamsal, L. N., Martin, R. V., van Donkelaar, A., Celarier, E. A., Bucsela, E. J., Boersma, K. F., Luo, R. D. C., and Wang, Y.: Indirect validation of tropospheric nitrogen dioxide retrieved from the OMI satellite instrument: insight into the seasonal variation of nitrogen oxides at northern midlatitudes, J. Geophys. Res., 115, D05302, doi:10.1029/2009JD013351, 2010. 14522, 14523, 14536, 14537, 14541, 14547

Lamsal, L. N., Martin, R. V., Padmanabhan, A., van Donkelaar, A., Zhang, Q., Sioris, C. E., Chance, K., Kurosu, T. P., and Newchurch, M. J.: Application of satellite observations for timely updates to global anthropogenic NO_x emission inventories, Geophys. Res. Lett., 38, L05810, doi:10.1029/2010GL046476, 2011. 14522, 14547

Lamsal, L. N., Martin, R. V., Parrish, D. D., and Krotkov, N. A.: Scaling relationship for NO_2 pollution and population size: a satellite perspective, Environ. Sci. Technol., 47, 7855–7861, 2013. 14522, 14535, 14547

Leitão, J., Richter, A., Vrekoussis, M., Kokhanovsky, A., Zhang, Q. J., Beekmann, M., and Burrows, J. P.: On the improvement of NO_2 satellite retrievals – aerosol impact on the airmass factors, Atmos. Meas. Tech., 3, 475–493, doi:10.5194/amt-3-475-2010, 2010. 14543

ACPD
14, 14519–14573, 2014

Levelt, P. F., van den Oord, G. H. J., Dobber, M. R., Malkki, A., Visser, H., de Vries, J., Stammes, P., Lundell, J. O. V., and Saari, H.: The ozone monitoring instrument, IEEE Trans. Geosci. Remote, 44, 1093–1101, 2006. 14524

Lin, J.-T.: Satellite constraint for emissions of nitrogen oxides from anthropogenic, lightning and soil sources over East China on a high-resolution grid, Atmos. Chem. Phys., 12, 2881–2898, doi:10.5194/acp-12-2881-2012, 2012. 14522

Lin, J.-T., McElroy, M. B., and Boersma, K. F.: Constraint of anthropogenic NO_x emissions in China from different sectors: a new methodology using multiple satellite retrievals, Atmos. Chem. Phys., 10, 63–78, doi:10.5194/acp-10-63-2010, 2010. 14522

Lu, Z. and Streets, D. G.: Increase in NO_x emissions from Indian thermal power plants during 1996–2010: unit-based inventories and multisatellite observations, Environ. Sci. Technol., 46, 7463–7470, doi:10.1021/es300831w, 2012. 14522

Martin, R. V., Chance, K., Jacob, D. J., Kurosu, T. P., Spurr, R. J. D., Bucsela, E., Gleason, J. F., Palmer, P. I., Bey, I., Fiore, A. M., Li, Q., Yantosca, R. M., and Koelemeijer, R. B. A.: An improved retrieval of tropospheric nitrogen dioxide from GOME, J. Geophys. Res., 107, 4437, doi:10.1029/2001JD001027, 2002. 14522

Martin, R. V., Jacob, D. J., Chance, K., Kurosu, T. P., Perner, P. I., and Evans, M. J.: Global inventory of nitrogen oxide emission constrained by space-based observations of NO_2 columns, J. Geophys. Res., 108, 4537, doi:10.1029/2003JD003453, 2003. 14522, 14536

Martin, R. V., Sioris, C. E., Chance, K., Ryerson, T. B., Bertram, T. H., Wooldridge, P. J., Cohen, R. C., Neuman, J. A., Swanson, A., and Flocke, F. M.: Evaluation of space-based constraints on global nitrogen oxide emissions with regional aircraft measurements over and downwind of eastern North America, J. Geophys. Res., 111, D15308, doi:10.1029/2005JD006680, 2006. 14522, 14547

McLinden, C. A., Fioletov, V., Boersma, K. F., Kharol, S. K., Krotkov, N., Lamsal, L., Makar, P. A., Martin, R. V., Veefkind, J. P., and Yang, K.: Improved satellite retrievals of NO_2 and SO_2 over the Canadian oil sands and comparisons with surface measurements, Atmos. Chem. Phys., 14, 3637–3656, doi:10.5194/acp-14-3637-2014, 2014. 14543

Mebust, A. K. and Cohen, R. C.: Observations of a seasonal cycle in NO_x emissions from fires in African woody savannas, Geophys. Res. Lett., 40, 1451–1455, doi:10.1002/grl.50343, 2013. 14522

ACPD
14, 14519–14573, 2014

Mebust, A. K., Russell, A. R., Hudman, R. C., Valin, L. C., and Cohen, R. C.: Characterization of wildfire NO_x emissions using MODIS fire radiative power and OMI tropospheric NO_2 columns, Atmos. Chem. Phys., 11, 5839–5851, doi:10.5194/acp-11-5839-2011, 2011. 14522

NARSTO: Improving emission inventories for effective air quality management across North America, A NARSTO Assessment, Tech. rep., NARSTO, available at: http://www.narsto.org/ (8 December 2013), 2005. 14523, 14536

Novotny, E. V., Bechle, M. J., Millet, D. B., and Marshal, J. D.: National satellite-based land-use regression: NO_2 in the United States, Environ. Sci. Technol., 45, 4407–4414, doi:10.1021/es103578x, 2011. 14522

Oetjen, H., Baidar, S., Krotkov, N. A., Lamsal, L. N., Lechner, M., and Volkamer, R.: Airborne MAX-DOAS measurements over California: testing the NASA OMI tropospheric NO_2 product, J. Geophys. Res., 118, 7400–7413, doi:10.1002/jgrd.50550, 2013. 14523

Olivier, J. G. J., Berdowski, J. J. M., Peters, J. A. H. W., Bakker, J., Visschedijk, A. J. H., and Bloos, J. P. J.: Applications of EDGAR. Including a description of EDGAR 3.2: Reference database with trend data for 1970–1995, Tech. rep., RIVM Bilthovan, RIVM report, Bilthovan, The Netherlands, 773301 001/NRP report 410200 051, 2001. 14547

Palmer, P. I., Jacob, D. J., Chance, K., Martin, R. V., Kurosu, T. P., Bey, I., Yantosca, R., Fiore, A. M., and Li, Q.: Air mass factor formulation for spectroscopic measurements from satellites: application to formaldehyde retrievals from the global ozone monitoring experiment, J. Geophys. Res., 106, 14539–14550, 2001. 14525

Palmer, P. I., Jacob, D. J., Fiore, A. M., Martin, R. V., Chance, K., and Kurosu, T. P.: Mapping isoprene emissions over North America using formaldehyde column observations from space, J. Geophys. Res., 108, 4180, doi:10.1029/2002JD002153, 2003. 14537

Park, R. J., Jacob, D. J., Field, B. D., Yantosca, R. M., and Chin, M.: Natural and transboundary pollution influences on sulfate-nitrate-ammonium aerosols in the United States: implications for policy, J. Geophys. Res., 109, D15204, doi:10.1029/2003JD004473, 2004. 14547

Piters, A. J. M., Boersma, K. F., Kroon, M., Hains, J. C., Van Roozendael, M., Wittrock, F., Abuhassan, N., Adams, C., Akrami, M., Allaart, M. A. F., Apituley, A., Beirle, S., Bergwerff, J. B., Berkhout, A. J. C., Brunner, D., Cede, A., Chong, J., Clémer, K., Fayt, C., Frieß, U., Gast, L. F. L., Gil-Ojeda, M., Goutail, F., Graves, R., Griesfeller, A., Großmann, K., Hemerijckx, G., Hendrick, F., Henzing, B., Herman, J., Hermans, C., Hoexum, M., van der Hoff, G. R., Irie, H., Johnston, P. V., Kanaya, Y., Kim, Y. J., Klein Baltink, H., Kreher, K., de Leeuw, G., Leigh, R., Merlaud, A., Moerman, M. M., Monks, P. S., Mount, G. H., Navarro-Comas, M.,

ACPD
14, 14519–14573, 2014

Oetjen, H., Pazmino, A., Perez-Camacho, M., Peters, E., du Piesanie, A., Pinardi, G., Puentedura, O., Richter, A., Roscoe, H. K., Schönhardt, A., Schwarzenbach, B., Shaiganfar, R., Sluis, W., Spinei, E., Stolk, A. P., Strong, K., Swart, D. P. J., Takashima, H., Vlemmix, T., Vrekoussis, M., Wagner, T., Whyte, C., Wilson, K. M., Yela, M., Yilmaz, S., Zieger, P., and Zhou, Y.: The Cabauw Intercomparison campaign for Nitrogen Dioxide measuring Instruments (CINDI): design, execution, and early results, Atmos. Meas. Tech., 5, 457–485, doi:10.5194/amt-5-457-2012, 2012. 14530

Platt, U.: Differential Optical Absorption Spectroscopy (DOAS), in: Air Monitoring by Spectroscopic Techniques, edited by: Sigrist, M. W., John Wiley, New York, USA, 27–84, 1994. 14525

Richter, A., Burrows, J. P., Nüß, H., Granier, C., and Niemeier, U.: Increase in tropospheric nitrogen dioxide levels over China observed from space, Nature, 437, 129–132, 2005. 14522

Ridley, B. A. and Grahek, F.: A small, low flow, high-sensitivity reaction vessel for NO chemiluminescence detectors, J. Atmos. Ocean. Tech., 7, 307–311, 1990. 14526

Ridley, B., Ott, L., Pickering, K., Emmons, L., Montzka, D., Weinheimer, A., Knapp, D., Grahek, F., Li, L., Heymsfield, G., McGill, M., Kucera, P., Mahoney, M. J., Schultz, M., and Brasseur, G.: Florida thunderstorms: a faucet of reactive nitrogen to the upper troposphere, J. Geophys. Res., 109, D17305, doi:10.1029/2004JD004769, 2004. 14526

Roscoe, H. K., Van Roozendael, M., Fayt, C., du Piesanie, A., Abuhassan, N., Adams, C., Akrami, M., Cede, A., Chong, J., Clémer, K., Friess, U., Gil Ojeda, M., Goutail, F., Graves, R., Griesfeller, A., Grossmann, K., Hemerijckx, G., Hendrick, F., Herman, J., Hermans, C., Irie, H., Johnston, P. V., Kanaya, Y., Kreher, K., Leigh, R., Merlaud, A., Mount, G. H., Navarro, M., Oetjen, H., Pazmino, A., Perez-Camacho, M., Peters, E., Pinardi, G., Puentedura, O., Richter, A., Schönhardt, A., Shaiganfar, R., Spinei, E., Strong, K., Takashima, H., Vlemmix, T., Vrekoussis, M., Wagner, T., Wittrock, F., Yela, M., Yilmaz, S., Boersma, F., Hains, J., Kroon, M., Piters, A., and Kim, Y. J.: Intercomparison of slant column measurements of NO_2 and O_4 by MAX-DOAS and zenith-sky UV and visible spectrometers, Atmos. Meas. Tech., 3, 1629–1646, doi:10.5194/amt-3-1629-2010, 2010. 14529

Russell, A. R., Valin, L. C., Bucsela, E. J., Wenig, M. O., and Cohen, R. C.: Space-based constraints on spatial and temporal patterns of NO_x emissions in California, 2005–2008, Environ. Sci. Technol., 44, 3608–3615, doi:10.1021/es903451j, 2010. 14522

Russell, A. R., Valin, L. C., and Cohen, R. C.: Trends in OMI NO_2 observations over the United States: effects of emission control technology and the economic recession, Atmos. Chem. Phys., 12, 12197–12209, doi:10.5194/acp-12-12197-2012, 2012. 14522

ACPD
14, 14519–14573, 2014

Ryerson, T. B., Williams, E. J., and Fehsenfeld, F. C.: An efficient photolysis system for fast-response NO_2 measurements, J. Geophys. Res., 105, 26447–26461, 2000. 14523
Schaub, D., Boersma, K. F., Kaiser, J. W., Weiss, A. K., Folini, D., Eskes, H. J., and Buchmann, B.: Comparison of GOME tropospheric NO_2 columns with NO_2 profiles deduced from ground-based in situ measurements, Atmos. Chem. Phys., 6, 3211–3229, doi:10.5194/acp-6-3211-2006, 2006. 14523
Schaub, D., Brunner, D., Boersma, K. F., Keller, J., Folini, D., Buchmann, B., Berresheim, H., and Staehelin, J.: SCIAMACHY tropospheric NO_2 over Switzerland: estimates of NO_x lifetimes and impact of the complex Alpine topography on the retrieval, Atmos. Chem. Phys., 7, 5971–5987, doi:10.5194/acp-7-5971-2007, 2007. 14522
Solomon, S., Portmann, R. W., Sanders, R. W., Daniel, J. S., Madsen, W., Bartram, B., and Dutton, E. G.: On the role of nitrogen dioxide in the absorption of solar radiation, J. Geophys. Res., 104, 12047–12058, 1999. 14521
Steinbacher, M., Zellweger, C., Schwarzenbach, B., Bugmann, S., Buchmann, B., Ordòñez, C., Prèvôt, A. S. H., and Hueglin, C.: Nitrogen oxides measurements at rural sites in Switzerland: Bias of conventional measurement techniques, J. Geophys. Res., 112, D11307, doi:10.1029/2006JD007971, 2007. 14523
Strahan, S. E., Duncan, B. N., and Hoor, P.: Observationally derived transport diagnostics for the lowermost stratosphere and their application to the GMI chemistry and transport model, Atmos. Chem. Phys., 7, 2435–2445, doi:10.5194/acp-7-2435-2007, 2007. 14525, 14546
Streets, D. G., Zhang, Q., Wang, L., He, K., Hao, J., Wu, Y., Tang, Y., and Carmichael, G. R.: Revisiting China's CO emissions after the Transport and Chemical Evolution over the Pacific (TRACE-P) mission: synthesis of inventories, atmospheric modeling, and observations, J. Geophys. Res., 111, D14306, doi:10.1029/2006JD007118, 2006. 14546
Tang, W., Cohan, D. S., Lamsal, L. N., Xiao, X., and Zhou, W.: Inverse modeling of Texas NO_x emissions using space-based and ground-based NO_2 observations, Atmos. Chem. Phys., 13, 11005–11018, doi:10.5194/acp-13-11005-2013, 2013. 14537
Thornton, J. A., Wooldridge, P. J., and Cohen, R. C.: Atmospheric NO_2: in situ laser-induced fluorescence detection at parts per trillion mixing ratios, Anal. Chem., 72, 528–539, doi:10.1021/ac9908905, 2000. 14526
Toenges-Schüller, N., Stein, O., Rohrer, F., Wahner, A., Richter, A., Burrows, J. P., Beirle, S., Wagner, T., Platt, U., and Elvidge, C. D.: Global distribution pattern of anthropogenic nitrogen

ACPD
14, 14519–14573, 2014

oxide emissions: Correlation analysis of satellite measurements and model calculations, J. Geophys. Res., 111, D05312, doi:10.1029/2005JD006068, 2006. 14537

Valin, L. C., Russell, A. R., Hudman, R. C., and Cohen, R. C.: Effects of model resolution on the interpretation of satellite NO_2 observations, Atmos. Chem. Phys., 11, 11647–11655, doi:10.5194/acp-11-11647-2011, 2011. 14542

van der A, R. J., Peters, D. H. M., Eskes, H., Boersma, K. F., Van Roozendael, M., De Smedt, I., and Kelder, H. M.: Detection of the trend and seasonal variation in tropospheric NO_2 over China, J. Geophys. Res., 111, D12317, doi:10.1029/2005JD006594, 2006. 14522

van der A, R. J., Eskes, H. J., Boersma, K. F., van Noije, T. P. C., Van Roozendael, M., De Smedt, I., Peters, D. H. M., Kuenen, J. J. P., and Meijer, E. W.: Identification of NO_2 sources and their trends from space using seasonal variability analyses, J. Geophys. Res., 113, doi:10.1029/2007JD009021, 2008. 14522

van Donkelaar, A., Martin, R. V., Leaitch, W. R., Macdonald, A. M., Walker, T. W., Streets, D. G., Zhang, Q., Dunlea, E. J., Jimenez, J. L., Dibb, J. E., Huey, L. G., Weber, R., and Andreae, M. O.: Analysis of aircraft and satellite measurements from the Intercontinental Chemical Transport Experiment (INTEX-B) to quantify long-range transport of East Asian sulfur to Canada, Atmos. Chem. Phys., 8, 2999–3014, doi:10.5194/acp-8-2999-2008, 2008. 14547

van Donkelaar, A., Martin, R. V., Pasch, A. N., Szykman, J. J., Zhang, L., Wang, Y., and Chen, D.: Improving the accuracy of daily satellite-derived ground-level fine aerosol concentration estimates for North America, Environ. Sci. Technol., 46, 11971–11978, doi:10.1021/es3025319, 2012. 14547

van Noije, T. P. C., Eskes, H. J., Dentener, F. J., Stevenson, D. S., Ellingsen, K., Schultz, M. G., Wild, O., Amann, M., Atherton, C. S., Bergmann, D. J., Bey, I., Boersma, K. F., Butler, T., Cofala, J., Drevet, J., Fiore, A. M., Gauss, M., Hauglustaine, D. A., Horowitz, L. W., Isaksen, I. S. A., Krol, M. C., Lamarque, J.-F., Lawrence, M. G., Martin, R. V., Montanaro, V., Müller, J.-F., Pitari, G., Prather, M. J., Pyle, J. A., Richter, A., Rodriguez, J. M., Savage, N. H., Strahan, S. E., Sudo, K., Szopa, S., and van Roozendael, M.: Multi-model ensemble simulations of tropospheric NO_2 compared with GOME retrievals for the year 2000, Atmos. Chem. Phys., 6, 2943–2979, doi:10.5194/acp-6-2943-2006, 2006. 14522, 14541, 14542

Vandaele, A. C., Hermans, C., Simon, P. C., Carleer, M., Colin, R., Fally, S., Merienne, M. F., Jenouvrier, A., and Coquart, B.: Measurements of the NO_2 absorption cross-section from 42 000 cm^{-1} to 10 000 cm^{-1} (238–1000 nm) at 220 K and 294 K, J. Quant. Spectrosc. Ra., 59(3–5), 171–184, 1998. 14528, 14530

ACPD
14, 14519–14573, 2014

Vinken, G. C. M., Boersma, K. F., van Donkelaar, A., and Zhang, L.: Constraints on ship NO_x emissions in Europe using GEOS-Chem and OMI satellite NO_2 observations, Atmos. Chem. Phys., 14, 1353–1369, doi:10.5194/acp-14-1353-2014, 2014. 14522

Wagner, N. L., Dubé, W. P., Washenfelder, R. A., Young, C. J., Pollack, I. B., Ryerson, T. B., and Brown, S. S.: Diode laser-based cavity ring-down instrument for NO_3, N_2O_5, NO, NO_2 and O_3 from aircraft, Atmos. Meas. Tech., 4, 1227–1240, doi:10.5194/amt-4-1227-2011, 2011. 14526

Wang, S., Pongetti, T. J., Sander, S. P., Spinei, E., Mount, G. H., Cede, A., and Herman, J.: Direct sun measurements of NO_2 column abundances from Table Mountain, California: intercomparison of low- and high-resolution spectrometers, J. Geophys. Res., 115, D13305, doi:10.1029/2009JD013503, 2010. 14530

Wang, S. W., Zhang, Q., Streets, D. G., He, K. B., Martin, R. V., Lamsal, L. N., Chen, D., Lei, Y., and Lu, Z.: Growth in NO_x emissions from power plants in China: bottom-up estimates and satellite observations, Atmos. Chem. Phys., 12, 4429–4447, doi:10.5194/acp-12-4429-2012, 2012. 14522, 14547

Wenig, M. O., Cede, A. M., Bucsela, E. J., Celarier, E. A., Boersma, F. K., Veefkind, J. P., Brinksma, E. J., Gleason, J. F., and Herman, J. R.: Validation of OMI tropospheric NO_2 column densities using direct-sun mode Brewer measurements at NASA Goddard Space Flight Center, J. Geophys. Res., 113, D16S45, doi:10.1029/2007JD008988, 2008. 14523

Zhang, L., Jacob, D. J., Smith-Downey, N. V., Wood, D. A., Blewitt, D., Carouge, C., van Donkelaar, A., Jones, D. B. A., Murray, L. T., and Wang, Y.: Improved estimate of the policy-relevant background ozone in the United States using the GEOS-Chem global model with $1/2^\circ \times 2/3^\circ$ horizontal resolution over North America, Atmos. Environ., 45, 6769–6776, 2011. 14547

Zhang, Q., Streets, D. G., He, K., Wang, Y., Richter, A., Burrows, J. P., Uno, I., Jang, C. J., Chen, D., Yao, Z., and Lei, Y.: NO_x emission trends for China, 1995–2004: the view from the ground and the view from space, J. Geophys. Res., 112, D22306, doi:10.1029/2007JD008684, 2007. 14522, 14547

Zhao, C. and Wang, Y.: Assimilation inversion of NO_2 emissions over east Asia using OMI NO_2 column measurements, Geophys. Res. Lett., 36, L06805, doi:10.1029/2008GL037129, 2009. 14522

ACPD
14, 14519–14573, 2014

Table 1. Aircraft flight parameters.

Site	Location type	Spirals	Minimum and maximum altitude (km)	Number of observations
Beltsville	suburban	43	0.24–2.03	19 867
Padonia	suburban	38	0.35–3.47	27 106
Fair Hill	rural	41	0.26–4.78	41 550
Aldino	rural/suburban	36	0.27–4.82	30 407
Edgewood	coastal/suburban	43	0.25–4.82	35 050
Essex	coastal/urban	38	0.24–3.26	30 269

ACPD
14, 14519–14573, 2014

Table 2. Summary of validation results.

Location	Data sources	Measurement period	Mean difference	Sample size
Beltsville, MD	P-3B	Jul 2011	−6.0 %	8
	Pandora		−5.9 %	8
Padonia, MD	P-3B	Jul 2011	−8.0 %	9
	Pandora		9.1 %	8
Fair Hill, MD	P-3B	Jul 2011	−22.1 %	8
	Pandora		43.9 %	8
Aldino, MD	P-3B	Jul 2011	−19.5 %	8
	Pandora		−5.4 %	7
Edgewood, MD	P-3B	Jul 2011	−41.3 %	10
	Pandora		−5.8 %	8
Essex, MD	P-3B	Jul 2011	−40.1 %	13
	Pandora		13.1 %	8
Hampton, VA	Pandora	2009–2011	−16.8 %	163
Tsukuba, Japan	MAX-DOAS	2006–2007, 2010–2011	−16.3 %	191
Hedo, Japan	MAX-DOAS	2007–2011	7.1 %	514
Yorkville, GA	In situ surface	2006–2009	−1.9 %	700
Centerville, AL	In situ surface	2006–2009	−17.8 %	676
Continental USA	NO_x emission inventory	2005	8.8 %	2706

ACPD
14, 14519–14573, 2014

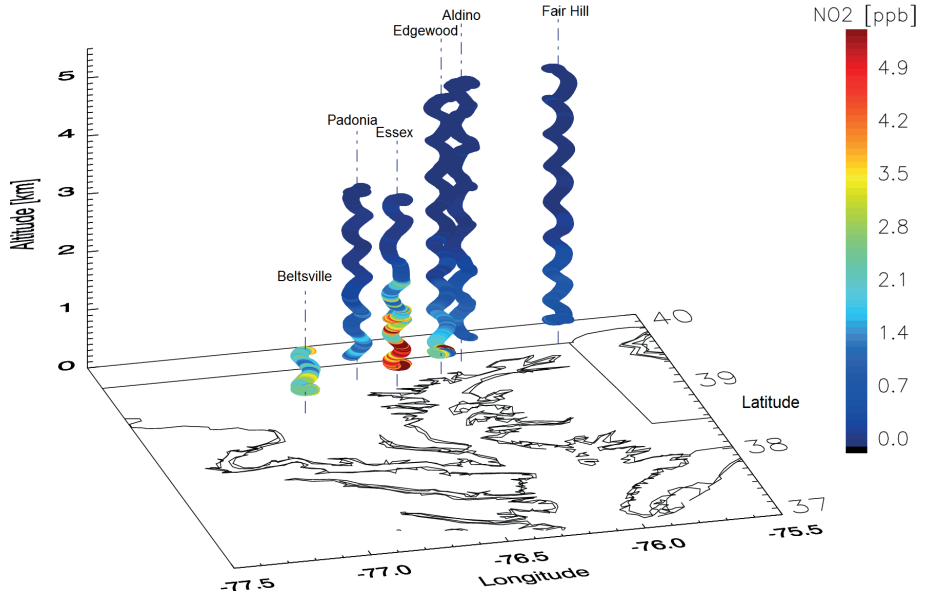

Figure 1. Distribution of NO_2 on 21 July 2011 obtained from P-3B aircraft measurements during the DISCOVER-AQ field campaign in Maryland. More than 190 000 1 s NO_2 measurements were taken during 254 spirals over the entire campaign period.

ACPD
14, 14519–14573, 2014

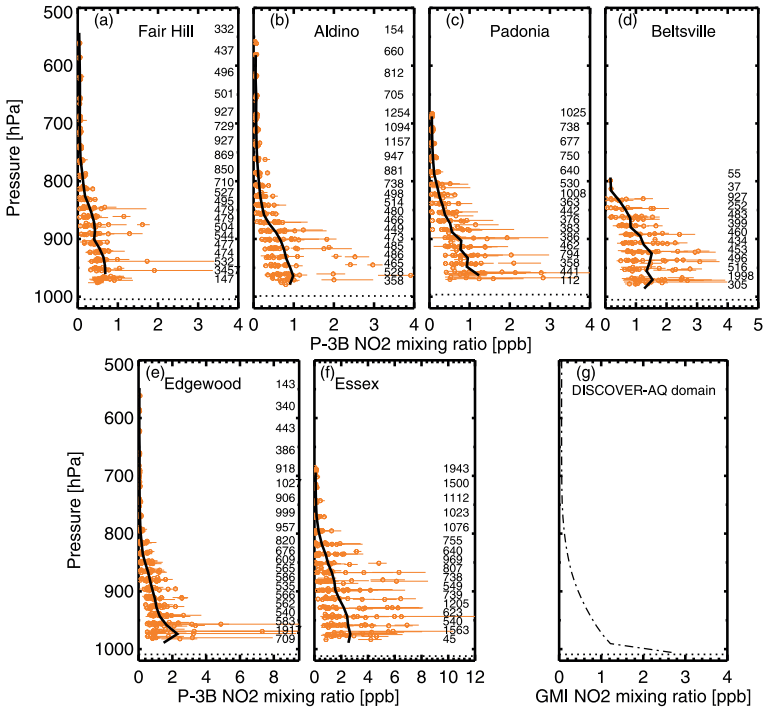

Figure 2. Early afternoon (12:00 to 15:00) vertical mean profile of NO_2 mixing ratio over Fair Hill, Aldino, Padonia, Beltsville, Edgwood, and Essex in Maryland. The open circles (in orange) represent NO_2 mixing ratios averaged over the GMI pressure grid from each spiral. Error bars represent the 10th to 90th percentiles. Solid black lines connect the mean mixing ratios determined from in situ measurements during the entire campaign. The number of measurements within each GMI pressure grid is shown in the right of each panel. The dotted lines show the surface pressure levels. The bottom-right panel shows the GMI a priori monthly (July) mean NO_2 mixing ratio profile over the DISCOVER-AQ domain.

ACPD
14, 14519–14573, 2014

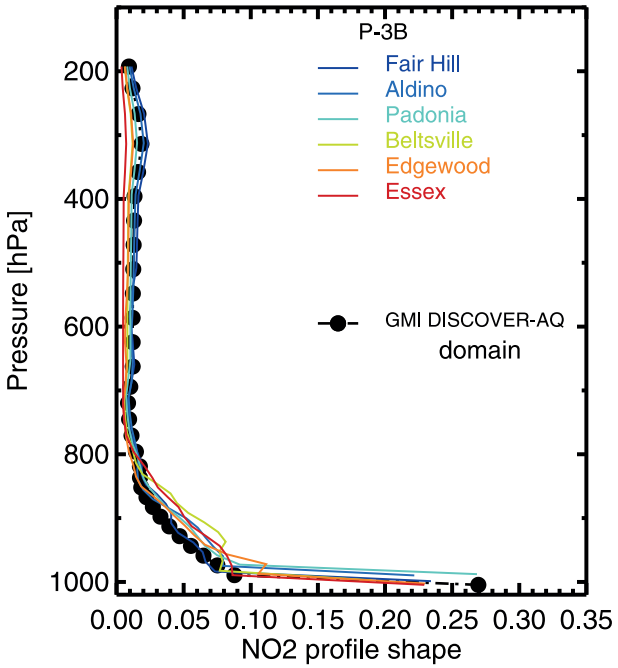

Figure 3. Relative vertical distribution (profile shape) of NO_2 over the six spiral locations during DISCOVER-AQ. The colored lines show the mean profile shapes determined from the in situ measurements. The shape factors are calculated as the ratio of partial columns to total tropospheric column. The dashed line with filled circles show the profile shape calculated from the GMI model.

ACPD
14, 14519–14573, 2014

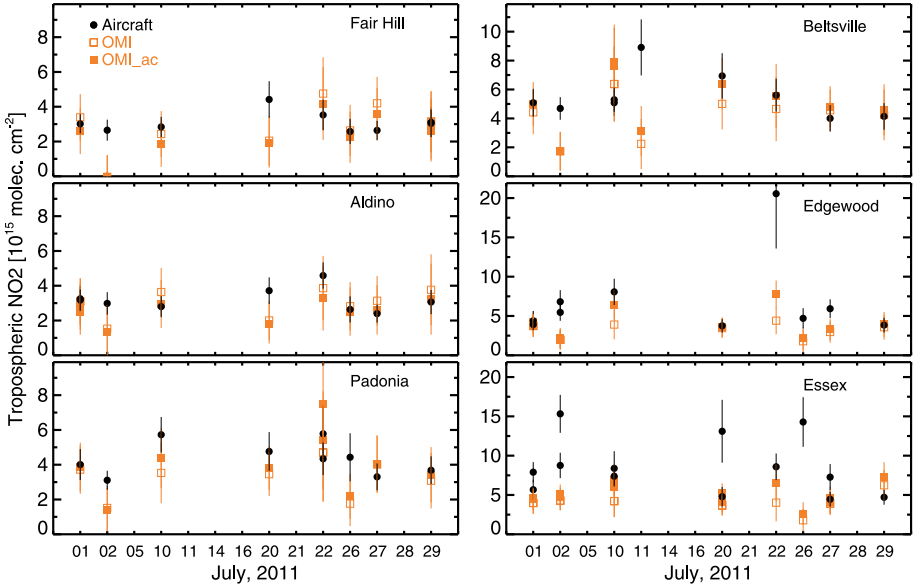

Figure 4. Comparison of tropospheric NO_2 columns retrieved from OMI (squares) with those determined from in situ measurements (filled circles). The figure shows OMI retrievals performed using GMI NO_2 a priori vertical profiles (open squares) and in situ NO_2 measurements (filled squares). Error bars represent errors in the aircraft measurements, extrapolated aircraft profiles, and OMI retrievals.

ACPD
14, 14519–14573, 2014

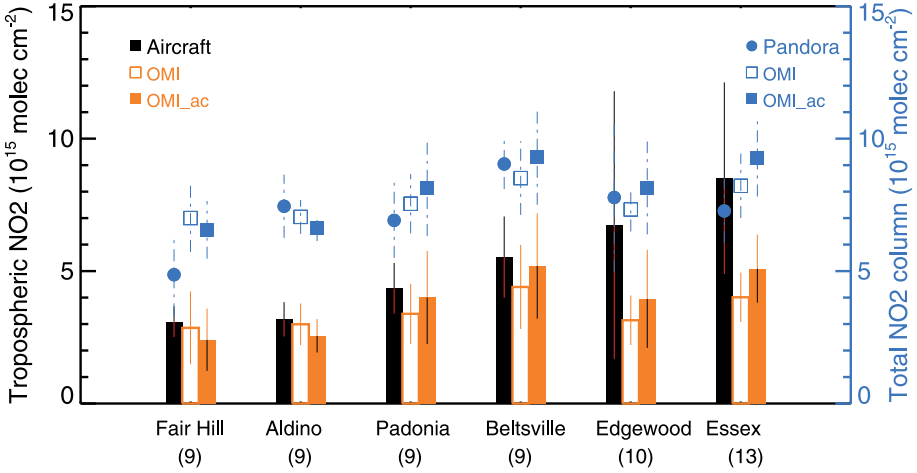

Figure 5. Comparison of average tropospheric (orange bars) and total (blue squares) NO_2 columns retrieved from OMI with tropospheric NO_2 columns determined from in situ aircraft (black bars) measurements and total columns retrieved from Pandora (filled blue circles) at the six locations in Maryland during the DISCOVER-AQ field campaign. Open bars and squares represent the operational retrievals and filled bars and squares represent the retrievals performed using collocated aircraft-measured NO_2 vertical profiles. The vertical lines represent the standard deviation of the average.

ACPD
14, 14519–14573, 2014

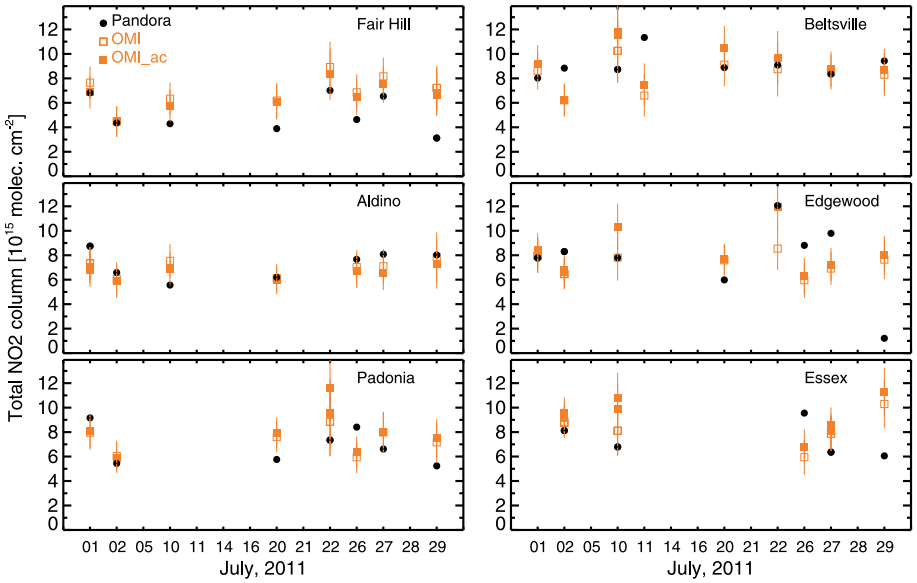

Figure 6. Comparison of total NO_2 columns retrieved from OMI (rectangles) with those retrieved from Pandora measurements (filled circles). Open squares represent the operational retrievals (using GMI profiles), and filled squares represent OMI retrievals performed using collocated aircraft-measured NO_2 vertical profiles. Error bars represent errors in Pandora and OMI retrievals.

ACPD
14, 14519–14573, 2014

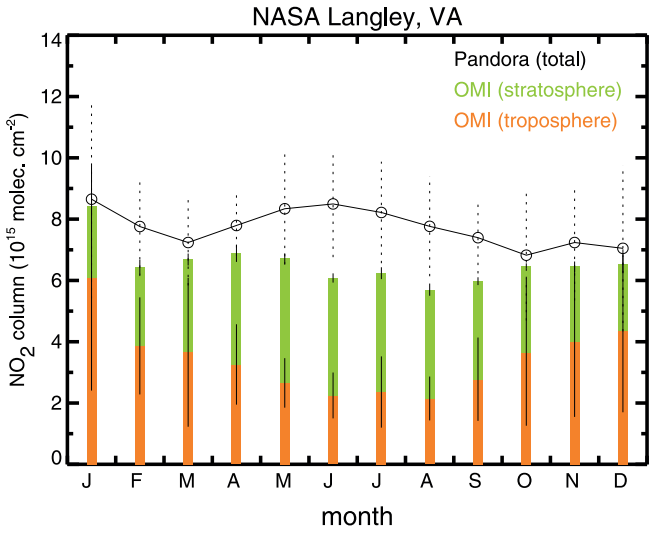

Figure 7. Monthly variation of total NO_2 columns at Hampton, VA for 2009–2012, as calculated from Pandora measurements (line with open circles) and OMI measurements (bars). OMI total NO_2 columns are separated into stratospheric (green bars) and tropospheric (orange bars) components. The bars represent the standard deviation of the average.

ACPD
14, 14519–14573, 2014

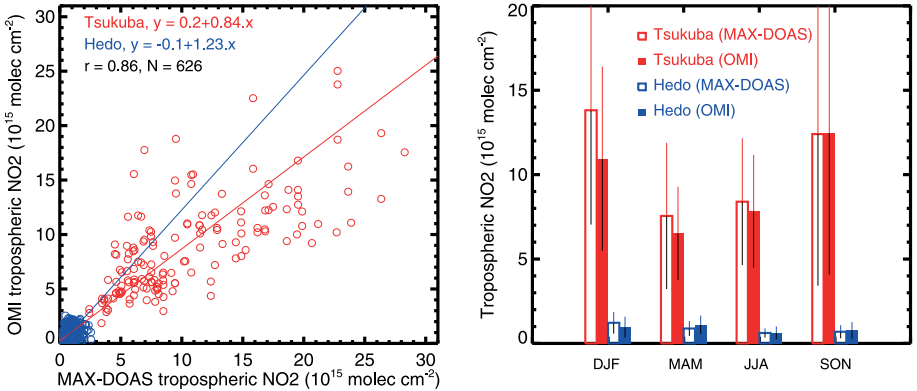

Figure 8. Comparison of tropospheric NO_2 columns retrieved from OMI and MAX-DOAS instruments. Observations at Tsukuba and Hedo, Japan, are shown in red and blue, respectively. (left) Scatter plot of OMI tropospheric NO_2 and MAX-DOAS measurements. The regression analysis parameters are given in the legend. The slope was calculated with reduced major-axis linear regression (Hirsch and Gilroy, 1984). (right) Seasonal mean tropospheric NO_2 columns for December–February (DJF), March–May (MAM), June–August (JJA), and September–November (SON) for 2006–2011 from MAX-DOAS (open bars) and OMI (filled bars). The vertical lines are the standard deviation of the seasonal average.

ACPD
14, 14519–14573, 2014

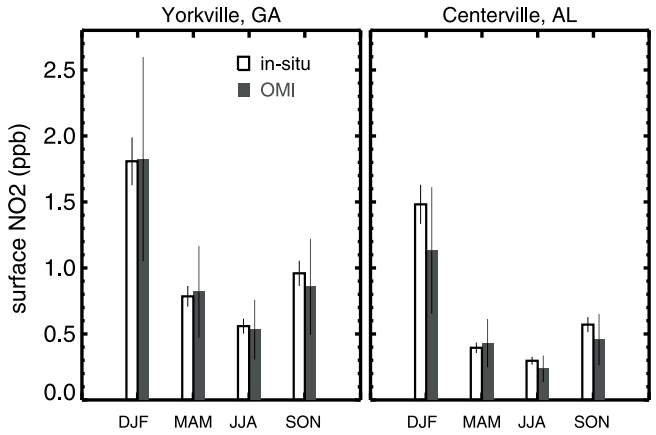

Figure 9. Seasonal variation of NO_2 mixing ratios at rural SEARCH sites for 2006–2010. Open bars represent seasonal mean NO_2 mixing ratios from in situ measurements, and solid bars represent those derived from the OMI tropospheric NO_2 columns. Error bars in in situ measurements represent 10 % errors in the photolytic converter measurements. Error bars in the OMI-derived surface NO_2 represent errors in retrievals including errors in the GEOS-Chem NO_2 profiles.

ACPD
14, 14519–14573, 2014

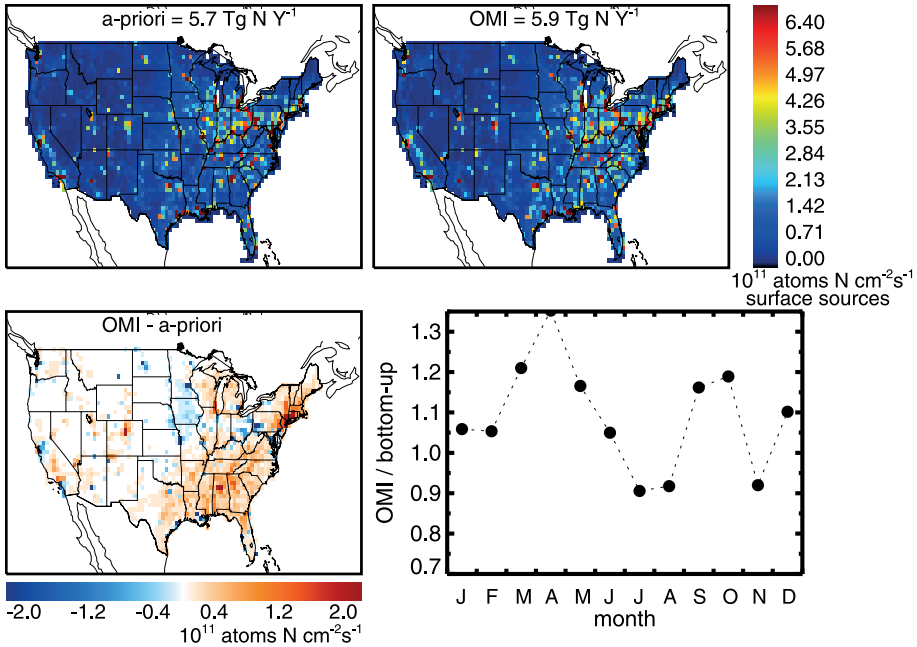

Figure 10. (top) Annual mean surface NO_x emissions over the United States for 2005. The left panel contains bottom-up emissions from fossil fuels, bio-fuels, biomass burning, and soils. The right panel shows top-down emissions estimated using OMI tropospheric NO_2 columns. The bottom left panel shows the difference between top-down and bottom-up surface NO_x emissions. (bottom right) Monthly mean ratio of area-averaged top-down surface NO_x emissions to bottom-up emissions over the United States.

ACPD
14, 14519–14573, 2014

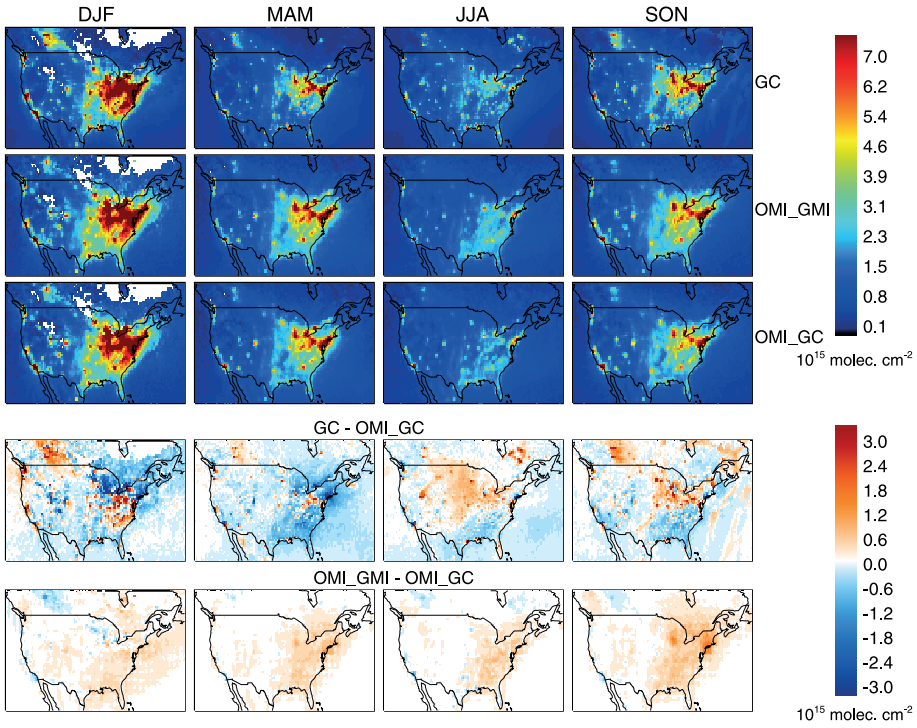

Figure 11. Seasonal mean tropospheric NO_2 columns binned at $0.5^\circ \times 0.667^\circ$ latitude × longitude over North America for 2005 from GEOS-Chem (first row), OMI standard product (OMI_GMI, second row), and OMI retrievals using the GEOS-Chem NO_2 a priori vertical profiles (OMI_GC, third row). White areas represent regions with insufficient data. The bottom two rows show the difference between (fourth row) GEOS-Chem and OMI_GC, and (fifth row) OMI_GMI and OMI_GC.

ACPD
14, 14519–14573, 2014